

Recent advances in the remote sensing of alpine snow: a review

Shubham Awasthi & Divyesh Varade

To cite this article: Shubham Awasthi & Divyesh Varade (2021) Recent advances in the remote sensing of alpine snow: a review, *GIScience & Remote Sensing*, 58:6, 852-888, DOI: [10.1080/15481603.2021.1946938](https://doi.org/10.1080/15481603.2021.1946938)

To link to this article: <https://doi.org/10.1080/15481603.2021.1946938>



Published online: 04 Aug 2021.



Submit your article to this journal



Article views: 2992



View related articles



View Crossmark data



Citing articles: 11 View citing articles



Recent advances in the remote sensing of alpine snow: a review

Shubham Awasthi ^a and Divyesh Varade ^b

^aCentre of Excellence in Disaster Management and Mitigation, Indian Institute of Technology Roorkee, Roorkee, India; ^bDepartment of Civil Engineering, Indian Institute of Technology Jammu, Jammu, India

ABSTRACT

Seasonal alpine snow contributes significantly to the water resource. It plays a crucial role in regulating the environmental feedback and from the perspective of socio-economic sustainability in the alpine regions. While most nations are pursuing renewable energy sources, hydropower generated from snowmelt runoff is one of the primary sources. Additionally, alpine regions with snow cover are major tourist destinations that are often affected by natural disasters such as avalanches. The snowmelt runoff and early avalanche warning require timely information on the spatio-temporal aspects of the snow geophysical parameters. In this regard, advances in remote sensing of snow have been observed to be significant. Recent developments in remote sensing technology in the visible, infrared, and microwave spectrum have significantly improved our understanding of snow geophysical processes. This paper provides a review concerning the qualitative and quantitative studies of alpine snow. The electromagnetic characteristics of the alpine snow are largely dependent upon its inherent geophysical structure and the properties of the snow. Snow behaves differently with respect to the wavelength of the incident radiation. In this paper, we provide a categorical review of the remote sensing techniques for estimating the snow geophysical properties, inclusive of permittivity, density, and wetness corresponding to the wavelength used in the remotely sensed data: (1) visible-infrared spectrum including multispectral/hyperspectral, (2) active and passive microwave spectrums. We also discuss the recent advancements in the remote sensing techniques for approximating the volumetric snowpack parameters such as the snow depth and the snow water equivalent based on active and passive microwave remote sensing. This review further discusses the limitations of the techniques reviewed and future prospects for the retrieval of snow geophysical parameters (SGP) corresponding to the recent progress in remote sensing technology. In summary, the recent advances have laid down a foundation for rigorous assessment of seasonal snow using spaceborne remote sensing, particularly at a regional scale. Yet, the scope for improvements in the methods and payload design exists.

ARTICLE HISTORY

Received 12 November 2020
Accepted 13 June 2021

KEYWORDS

Snow; remote sensing; liquid water content; snow density; snow depth

1. Introduction

Snow is an essential component of the cryosphere and has an essential role in maintaining the Earth's energy budget and global temperature. Investigations of the alpine snow are significant for climate and environmental modeling. Additionally, the extent and the volume of the alpine snow is also an indicator of global climate change and is often used in climate change modeling (Aguirre et al. 2018). Snow cover has a considerable influence on the land surface albedo. Snow covers annually, on average, an area of 46 million square kilometers (about 17.8 million square miles) around the world (Snow and Climate | National Snow and Ice Data Center). Snow has a higher surface albedo than

other land cover types (You et al. 2020). Snow reflects around 80% to 90% of the sun's energy into the atmosphere, providing a considerable feedback effect in a warming climate and helping to regulate the exchange of heat between the Earth's surface and the atmosphere (Bellaire, Jamieson, and Fierz 2011). Changes in the snow cover extent can largely affect the regional temperature and moisture interactions of the land and atmosphere, hence affecting the Earth's energy budget (Joshi et al. 2015).

The alpine regions exhibit a snow-free season where the soil layer is exposed, while the Polar Regions are typically covered in ice (Brown and Robinson 2005; Bokhorst et al. 2016; Callaghan et al. 2011; Wipf and Rixen 2010). The precipitation in alpine regions generally falls on the windward-

facing mountain slopes because of the dynamics associated with the uplift. Since most of the moisture is extracted from the clouds on the windward slopes, the air that crosses over to the lee side of the mountains is essentially dry (Barros and Lettenmaier 1994; Jiang 2003; Singh, Ramasastri, and Kumar 1995; Siler and Roe 2014). In the case of alpine snow, the underlying layer comprises soil, while for Polar Regions, the underlying layer of snow comprises ice often including some level of salinity (Anisimov et al. 2007; White and McCallum 2018). Furthermore, the temperature regime observed in the alpine snow affects its properties distinctly as compared to polar snow (Anisimov et al. 2007; Xie et al. 2017; Bender, Lehning, and Fiddes 2020). These factors typically lead to the differences in the physical properties of alpine and polar snow.

The snowfall and the regional temperature affect the revenue generated by the winter tourism industry, particularly in the mountain and foothills region, significantly affecting the socio-economic development in the area (Pütz et al. 2011). Climate change and the abnormal fluctuations in the climate can cause potential losses to this tourism industry (Töglhofer, Eigner, and Prettenthaler 2011). Advanced prediction of the snowfall variability in these regions during the winter season can be helpful in estimating the probable number of tourists visiting the region (Pütz et al. 2011). This can provide substantial opportunities to the authorities for facilitating adequate infrastructure arrangements.

Seasonal snow cover constitutes nearly one-sixth of the world's freshwater needs (Mithen and Black 2011). The available freshwater through rivers in alpine regions is usually a combination of snowmelt runoff and glacial discharge (Bernier et al. 2017). For example, in the Himalayas, these rivers serve the freshwater demands of nearly 1.4 billion people across several countries. Further, these rivers also significantly contribute to hydropower generation (DeBeer and Pomeroy 2017). The amount of liquid water present within the snowpack volume that should be released when the snowpack melt is represented as snow water equivalent (SWE) (Bookhagen and Burbank 2010). SWE is determined by snow depth, snow density, snow type, previous freeze/thaw cycles, and recent snowfall events, etc. (Yao et al. 2018). Therefore, proper estimation and prediction of SWE and snowmelt runoff are crucial for

studying the catchment hydrological behavior for water resource management (Kirkham et al. 2019). The snowmelt runoff is a major component of the fresh water. It is a regulator of the seasonal discharge to the rivers and often potential flooding (Jeelani et al. 2012). The volume and timing of snowmelt runoff depend on the air temperature, snow water equivalent, and melting of the snow (Johnston and Smakhtin 2014). Snowmelt depends on the internal temperature of the snowpack, surface albedo, snowpack density, and atmospheric factors like wind, relative humidity, temperature, and insolation (Akhtar, Ahmad, and Booij 2008). The variation in these parameters with climate change affects the amount and timing of the snowmelt runoff (Fischer 2013; Li et al. 2019).

Avalanches constitute one of the dominant and most severe natural hazards from the perspective of loss of human lives, infrastructure, and resources. Avalanches are usually triggered by snowpack rupture due to intolerable mechanical stresses acting in the snowpack. Often, avalanches are induced by the variations in the snow geophysical parameters (SGP), including the snow density, liquid water content (wetness), depth, grain size, etc., and meteorological parameters (Baggi and Schweizer 2009). Therefore, timely information on the spatial and temporal variation of the SGP has been deemed to be critical for avalanche zonation and forecasting (Steinkogler, Sovilla, and Lehning 2014). Further, this information is also significant toward closing the gap between the implementation of dynamic simulations for short-term avalanche hazard assessment and susceptibility mapping (Bellaire et al. 2017). It is evident that the observations of the SGP are essential for precisely estimating the potential areas of avalanche runouts that negatively affect the transportation infrastructure, including roads, railway networks, and human settlements (Fischer 2013).

Traditionally, the most accurate information on the SGP is available from the field measurements from intrusive physical equipment (which disturb snowpack) such as snow tubes or snow wedges (Kinar and Pomeroy 2015). However, this information is obtained as point measurements that are insufficient to derive inferences on the spatial distribution of the SGP (Ellerbruch and Boyne 1980). Furthermore, the field campaigns for collecting the SGP measurements are constrained by numerous hindrances, including

but not limited to the immediate weather conditions, available human resources, logistics, and infrastructure, particularly in the Himalayas, etc. (Thakur et al. 2016). The utilization of remote sensing techniques accounts for these issues and plays a significant role in determining spatially distributed information on snow and SGP (Dietz et al. 2012; Thakur et al. 2012).

The purpose of this review is to provide an overview of the application of satellite remote sensing for the characterization of the alpine snowpack. The focus of the review is to provide an overview of the remote sensing techniques utilizing the optical and microwave properties of the snowpack for deriving the key snow geophysical parameters like snow depth, snow density, snow wetness, etc. An overview of the alpine snowpack properties is initially described to enable the readers with a brief background of the snow surface and volume processes in the alpine regions. This review answers the following questions and is organized as follows.

- An introductory discussion for understanding the significance of the studies of the alpine snowpack, i.e. why are we interested in studying the alpine snowpack?
- A background on the snow metamorphism processes and traditional field practices for snow studies in alpine regions. How the alpine snowpack evolves seasonally, and how is it measured or quantified?
- A background on the geophysical, optical, and microwave properties of snow. How does snow behave corresponding to the different wavelengths of the electromagnetic spectrum?
- An overview of the various remote sensing methods for qualitative remote sensing of snow. What are the different remote sensing methods in the literature and their basis for qualitative studies of snow?
- An overview of the various methods for the quantitative determination of the snowpack geophysical parameters. How remote sensing is used in the quantitative determination of snowpack geophysical parameters.
- A discussion on the challenges and issues associated with the different remote sensing techniques for the studies of the alpine snowpack. What are the challenges that the research community needs to address in the future for

applying the various remote sensing techniques for the studies of alpine snow, and what are the future prospects in this regard?

A conclusion section completes the review by summarizing the role of remote sensing technology for snowpack monitoring and the future directions for the related developments.

2. Snow metamorphism and snow measurements in alpine regions

2.1. An overview of the snowpack

The snowpack comprises several layers of snow that accumulate through a series of snowfall events. Each of the snow layers naturally comprises a mixture of ice particles, air, and water, with the proportion of these components depending upon the atmospheric conditions and the age of snow. The stratigraphy of snow is defined by the profiles for the varying properties of the snow layers and their boundaries in the snowpack (Singh, Singh, and Haritashya 2011). The stratigraphic methods that are conventionally used are broadly based on (Pielmeier and Schneebeli 2003): (1) verbal interpretation of the snowpack stratigraphy; (2) optical recordings (analog and digital) of the stratigraphy; (3) morphology with respect to the shape and grain size of the snow particles; (4) mechanical properties (microstructure) of the snowpack layers; (5) texture of the snowpack layers combining the morphological and mechanical aspects; (6) dielectric properties of the snowpack layers. These aspects (3–6) of the snowpack are often characterized by the SGP (Baggi and Schweizer 2009; Najibi and Jin 2013).

2.2. Snow metamorphism in alpine snow

As compared to the polar regions, in the alpine regions, temperature declinations are typically with respect to the increasing elevation, introducing significant spatial variability. Often, these variations cause variability in the physical properties of snow. The Alpine snow microstructure undergoes substantial changes due to the thermodynamic transformations (McGregor 1990). Fresh snow comprises a branched structure with a hexagonal pattern of protruding vertices. The fresh snow particles start decaying as soon as they interact with the Earth's

surface. Typically, three types of metamorphism have been described in the literature (Singh, Singh, and Haritashya 2011); (1) Equilibrium or Equi-temperature (ET) forms, (2) Temperature gradient (TG) forms, and (3) Melt-freeze (MF) forms. The ET or the TG forms are dependent upon the temperature and the temperature gradients in the snowpack layers and cause rounding of the snow grains. In the ET form, the snow grains undergo a variety of shape transformation while finally settling into an equidimensional round shape. The water molecules in this case move largely by the diffusion of vapor to new positions to reduce the free surface energy. Typical fresh snow in the atmosphere occurs in the form of dendrites, needles, etc., with a large surface-to-area ratio and subsequently higher free surface energy per unit mass. During the equi-temperature metamorphism, there is a continuous decrease of this surface energy due to vapor transitions (Sommerfeld and LaChapelle 1970). The TG forms are usually observed in shallow snowpack with low air temperatures that are typically observed in the early winter season in the alpine regions. The differences in the internal temperatures of the snowpack layers cause the vapor migration from high to low-temperature regions in the snowpack. The vapor migration occurs continuously till the gradient is maintained. When obstructed by snow grains, the vapor settles down on the snow grain faces and causes incurvation of the snow grains (Sommerfeld and LaChapelle 1970). An example of water vapor transport from warmer temperatures to colder regions of the snowpack is the formation of the depth hoar (sugary crystals arranged in a fluffy layer). Such a shape renders the snowpack vulnerable to shear forces like the winds (Singh, Singh, and Haritashya 2011). The MF processes are defined by the periodical variations in the snow skin temperatures resulting in the formation of large polygranular grains after repeated cycles of melt and refreeze. Such processes are particularly prominent in the mid-winter seasons in the alpine regions (Colbeck 1982).

2.3. Field measurement practices of snow

Historically, snowpack properties are assessed based on in-situ measurements collected by devices that are categorized in several ways, the most basic being portable or stationary. Traditionally, the stationary devices are used in continuous monitoring for the

studies of snowpack evolution (Kinar and Pomeroy 2015). In contrast, portable devices are typically also used for the validation of different techniques developed for the estimation of snow geophysical parameters. The mechanical devices used for snow depth and SWE measurements are typically, rulers, depth rods, snow wedges, snow tubes, etc. Typically, for measuring the SWE, snow tubes are commonly used (Kinar and Pomeroy 2015).

Snow pit measurements or stratigraphic measurements of snow are typically carried out using electronic devices such as the Snow Fork or the Denoth meter. The Snow Fork, as the name suggests, comprises a two-pronged waveguide that operates at a resonant frequency range between 500 and 900 MHz and measures both the real and the imaginary parts of the permittivity (Sihvola and Tiuri 1986). The imaginary part of permittivity is significant for studying the extinction coefficient of the incident microwave signal. The Snow Fork needs to be calibrated before usage in the air-snow medium (Techel and Pielmeier 2011). The Denoth meter is a capacitive probe that measures the permittivity of snow. It comprises a flat plate antenna of 900 sq. cm corresponding to a $4 \times 15 \times 15 \text{ cm}^3$ cuboid with an effective area of measurement of 176 cm^2 (Kinar and Pomeroy 2015). Considering that snow comprises air, ice, and liquid water molecules, the snow wetness, which is the fraction of liquid water present in the snow, is a function of the snow permittivity and the snow density. Thus, the Denoth meter requires an alternative measurement of density to determine the liquid water content (LWC) (Denoth 1994). The Denoth meter gives only the real part of permittivity but is known to be slightly more precise than the Snow Fork (Techel and Pielmeier 2011).

3. Electromagnetic properties of snow

3.1. Optical properties of snow

3.1.1. Spectral differentiation of snow from other targets

In the visible and infrared spectrum, snow has significantly different reflectance as compared to several other materials. The spectral signature of snow is characterized by a very high reflectance in the visible spectrum followed by a lower reflectance in the short wave infrared (SWIR) spectrum (Hall, Riggs, and

Salomonson 1995). Figure 1 shows the comparison of spectral signatures of snow and other earthly features based on Advanced Spaceborne Thermal Emission Reflection Radiometer (ASTER) spectral library, the ASTER spectral library (Baldridge et al. 2009). In contrast to snow, other similar materials such as ice and water have much lower reflectance. The high reflectivity in the visible spectrum and the higher absorption coefficient in the SWIR spectra around the 1.5 μm and 2.0 μm contribute to the concept of identification of snow using the Normalized Difference Snow Index (NDSI) (Hall, Riggs, and Salomonson 1995). The NDSI is generally defined as the ratio of the difference to the sum of the reflectance in the green and SWIR bands. Although clouds also exhibit a higher reflectance in the visible spectrum, these contrastingly exhibit relatively higher reflectance in the SWIR spectrum and thus, can be differentiated from snow. However, thin cirrus clouds are an exception that exhibit similar spectral response in the entire visible and infrared spectrum to snow (Bian et al. 2016).

3.1.2. Spectral characterization of snow

The freshly fallen snow appears in the form of a powdered material comprising ice and air with a very low density and fine grain size. As the snow gets old, the atmospheric processes result in particles that cling to each other, increasing the snow grain size and density (Meløysund et al. 2007). This process also often occurs due to the presence of LWC in the snowpack (Colbeck 1982). Subsequently, the spectral reflectance of snow reduces throughout the visible and infrared spectrum. As compared to snow, ice and water are good absorbers of light, implying that they absorb the incident energy significantly at all wavelengths of the visible and infrared spectrum. Thus, differentiating snow is relatively easier from ice and water (Shekhar et al. 2019). Furthermore, characterizing the snow with respect to the snow grain size is also possible based on indices such as the snow grain index (Chang et al. 1976), which utilizes the spectral observations of the visible and near-infrared (NIR) reflectance. Dozier (1989) proposed four indices using Landsat Thematic Mapper band reflectances (R_λ) for deriving qualitative inferences on snow contamination and snow grain size. For differentiating contaminated snow and uncontaminated snow, a normalized and differenced index based on blue and green wavelengths was proposed. The other

three indices utilized the reflectance in blue, NIR, SWIR wavelengths in different normalized differenced combinations. However, these three indices do not discriminate the grain size irrespective of the contamination and are generic in nature. Further, these relations do not apply to refrost snow. Since the refrost snow and the wet snow typically have similar grain sizes and reflectance, except in the 0.98 to 1.3 μm region, where the absorption coefficient shifts from the water to the ice (Dozier et al. 2009). Thus, for the precise monitoring of spatio-temporal variability of wet or refrost snow, we require hyperspectral data with bands in the 0.98 to 1.3 μm region of the infrared spectrum. Figure 2 shows the spectral reflectance curves for the snow comprising different grain sizes, frost, ice, and water.

3.1.3. Thermal properties of snow

In contrast to earth materials, the emissivity of water is relatively high, and the more the absorption, the higher the emissivity. Figure 3(a) shows the emissivity response curves for some materials. At 300 K, the Earth radiates maximum energy at a peak wavelength of 9.66 μm , at which the emissivity of snow and ice is significantly larger than earthly materials (Snyder 1997). The higher emissivity of snow indicates the effect of the global snow cover in regulating the climate and the planetary energy budget of Earth (Vavrus 2007; Yu, Liu, and Zhang 2017). Among the different forms of water, the emissivity of snow is higher than that of water and ice. Figure 3(b) shows the emissivity of some samples collected at the Mammoth Mountains in California, United States. It is observed that the spectral emissivity of the snow samples is relatively higher than for water or ice.

3.2. Microwave interaction with snowpack

At a given microwave frequency, the relative proportion of the liquid water and ice in the snowpack decides the dielectric properties of the snow (Ulaby et al. 1977). This liquid water is responsible for the absorption of microwaves in a snowpack. The dielectric properties of a medium are represented by the complex relative permittivity or dielectric constant (ϵ_r) and is defined as $\epsilon_r = \epsilon'_r - j\epsilon''_r = n^2$, where n is the complex refractive index of the medium. The overall dielectric constant of the snowpack is the function of

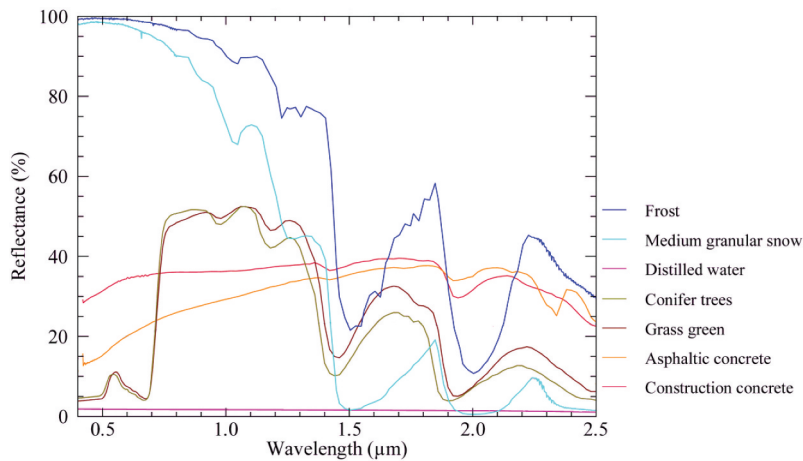


Figure 1. Comparison of spectral signatures of snow and other earth features based on ASTER spectral library data (Baldridge et al. 2009).

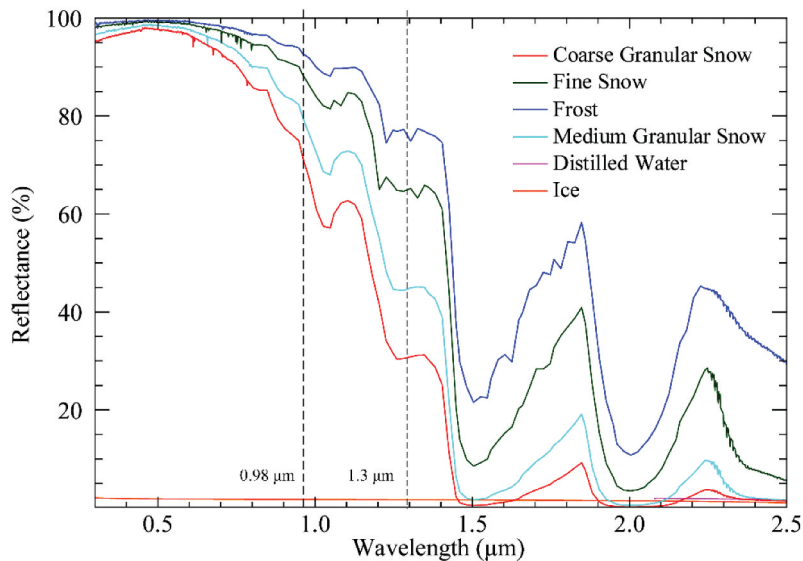


Figure 2. Comparison of the spectral signatures of snow for different types of grain sizes with water, frost, and ice (Baldridge et al. 2009).

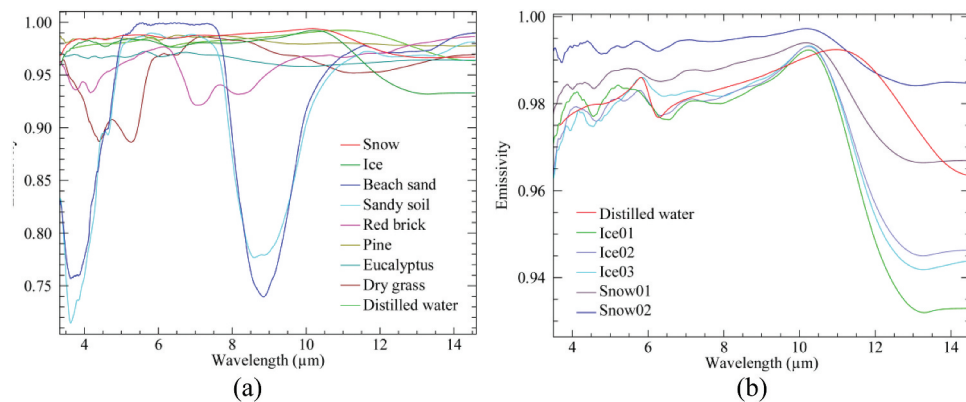


Figure 3. Emissivity response for different wavelengths for (a) various materials (Wan, Ng, and Dozier 1994; Snyder 1997), (b) snow, ice, and water (Wan, Ng, and Dozier 1994).

snowpack LWC, operating frequency of the microwave, surrounding temperature, and snowpack density (Stiles and Ulaby 1981). Here, the real part ϵ'_r of the snowpack is responsible for the refraction, scattering, and transmission of the EM waves in the snowpack. For dry snow, the real part of the dielectric constant is the function of snow density (ρ) represented as is related to the empirical relationship as given in equation (1). It shows a very weak dependence on the temperature.

$$\epsilon'_r = 1 + 1.5995\rho_s + 1.861\rho_s^3 \text{ for } \rho_s \leq 0.5 \text{ g/cm}^3 \quad (1)$$

The overall snow density varies from 0.05 g/cm³ (freshly fallen) to 0.5 g/cm³ (Looyenga 1965; Shi, Xiong, and Jiang 2016). For the dry snow ($\rho = 0.5 \text{ g/cm}^3$), the maximum value of ϵ''_r comes as 1.63. The imaginary part of the snowpack dielectric constant (ϵ''_r) is also termed as the dielectric loss (Kontu et al. 2020). The imaginary part of the dielectric constant (ϵ''_r) of the snowpack defines the absorption or extinction of the microwave in the snowpack. ϵ''_r is related to the operating frequency of the signal, temperature, and snowpack density. An empirical model relating ϵ''_r and the frequency (f) for the range (2–20 GHz) is given by $\epsilon''_r = (A/f + Bf^C)$, where A , B , and C are temperature-dependent parameters. Alternatively, ϵ''_r can be defined as shown in equation (2). This relationship is applicable for the frequency range between 0.8 GHz – 12 GHz and the temperature range of 0° C to –30° C (Dozier 1989).

$$\begin{aligned} \epsilon''_r &= 1.59 \\ &\times 10^6 (0.52 + 0.62\rho^2) \cdot \left(\frac{1}{f} + 1.23 \times 10^{-14} \sqrt{f} \right) e^{0.036T} \end{aligned} \quad (2)$$

The microwave absorption in the snowpack increases with increasing temperature and decreases with increasing frequency. It is evident that an increase in absorption causes a decrease in the penetration depth of the microwave in the snowpack. For a 20 GHz microwave signal, the penetration depth is approximately 1 m (Derkens, Walker, and Goodison 2003; Tsang et al. 2008). The penetration of the incident EM wave in the snowpack depends on the extinction coefficient (k_e) of the snowpack. Here, k_e represents the sum of the volume absorption coefficients (k_a) and the volume scattering coefficient (k_s

(Montpetit et al. 2013; Maslanka et al. 2019; Saberi et al. 2020). The imaginary part of the snowpack dielectric constant (ϵ''_r) regulates this absorption coefficient (k_a), and the scattering coefficient (k_s) depends on the geometry and the inhomogeneities of the snowpack with respect to the wavelength of the incident wave (Leinß and Hajnsek 2012).

The homogenous snowpack consists of densely packed, randomly distributed point scatterers of ice, all having the same geometry and dielectric. However, the seasonal snowpack usually contains inhomogeneities corresponding to the shape and size of the ice particles and different dielectric properties of the individual layers. The penetration depth (d_p) for the snowpack is defined as the depth where the power of the incident wave is damped by a factor of $1/e$ of the initial power (Pardé, Goïta, and Royer 2007), where e is constant (~2.72, natural/Euler number). This penetration depth is inversely proportional to the extinction coefficient (k_e) given as $d_p = k_e^{-1}$. The retrieval of k_e at a microwave frequency (f) requires information on the average grain size (d_o) of the snowpack; $k_e = 0.0018f^{2.8}d_o^2$ (Hallikainen, Ulaby, and Van Deventer 1987). The penetration depth of the incident wave within the snowpack can be defined in terms of the real and imaginary part of the snowpack dielectric constant (neglecting the effect of k_s) and wavelength of the incident wave as presented in equation (3) (Tsang et al. 2016).

$$d_p = \frac{\lambda_0 \sqrt{\epsilon'_r}}{2\pi\epsilon''} \quad (3)$$

3.2.1 Backscattering from snowpack

The backscatter from the snowpack depends on various snow-layer properties. The backscatter from the snowpack is affected by the quasi-horizontal layering of snow. Variation in the snow properties like snow density and dielectric constant is typically observed in various stratigraphic layers of the snowpack (Strozzi, Wiesmann, and Mätzler 1997; Matzler et al. 1997; Nagler et al. 2016). A significant effect of this stratigraphic variation is observed on the backscatter of the snowpack. The effect of stratigraphy is very less for the backscattering from the wet snow due to low penetration depth (Nagler 1996; Singh and Venkataraman 2010). Typically, the backscattering from the snowpack is categorized under the two-layer (air-snow and the snowpack volume) boundary

problem (Chang et al. 1996). The EM wave incident on the snowpack surface is partially, reflected, and transmitted through to the snowpack volume. The transmitted wave inside the snowpack layer is attenuated by the absorption and scattering losses inside the snowpack medium (Nagler 1996; Iru et al. 1998; Nagler and Rott 2000).

The total backscattering from the snowpack comprises components from the air–snow interface, the snowpack volume, and the snow–ground interface (Shi, Xiong, and Jiang 2016; Singh et al. 2017). The proportion of the scattering power for each of the components varies corresponding to the state of the snowpack and its thickness. The surface scattering from the snowpack is also dependent upon the surface roughness, which in general is low as the surface is usually considered to be bare smooth except in cases of Sastrugi or disturbed snow (Leroux and Fily 1998; Zhuravleva and Kokhanovsky 2011). The surface roughness properties are determined by various statistical components of the surface height like surface correlation length, the standard deviation of the surface height variation, and the correlation function shape (Ulaby, Moore, and Fung 1981; Ulaby et al. 2014). The scattering from the snowpack particles and the absorption coefficients are used to determine the attenuation of the microwave in the snowpack (Nagler 1996; Kokhanovsky and Zege 2004). In practice, the scattering coefficients are determined by the snow particle size and wavelength of the incident wave, and the absorption coefficients are determined by the dielectric constant of the snowpack and LWC (Tiuri et al. 1984; Grody 2008).

The Synthetic Aperture Radar (SAR) backscatter from the wet and dry snow shows a high variation due to the dissimilarity in the dielectric properties and the penetration depths (Hallikainen 1992). The snowpack above 0 °C is often considered as the wet snow, and the snowpack at the temperatures below 0 °C LWC nearly <1% by volume is considered as the dry snow (Stiles, Ulaby, and Rango 1981; Ulaby et al. 1982; Thakur et al. 2016). In dry snow, the dominant backscattered power comprises contributions from the volume scattering of the snowpack and the scattering components from the snow/ground interface. When the dry snow becomes old, the surface component from the air–snow interface also upsurges due to the increase in the snow grain size because of the melting and refreezing of the top layer of the

snowpack (Shi and Dozier 1995; Yueh et al. 2009; Varade et al. 2020a). The backscatter from the wet snowpack has a stronger surface component and weaker volume component and, typically, no component from the snow–ground interface (Thakur et al. 2012). For the same snowpack thickness, generally, the dry snow backscatter is higher than that for wet snow (Shi and Dozier 1995; Nagler and Rott 2000; P. K. Thakur et al. 2013; Awasthi et al. 2020).

In general, the backscatter response of the snowpack is influenced by various factors such as the radar wavelength, polarization of the wave, incidence angle (θ_i), local incidence angle (θ_l), surface roughness, and dielectric properties (Baghdadi and Zribi 2006; Fung and Chen 2010; Ulaby et al. 2014). The radar waves of shorter wavelengths experience higher backscattering compared to the longer wavelengths from the snowpack. The dry snowpack of grain size in the range 0.1 to 0.3 mm is transparent for radar waves of longer wavelength. The transparency implies that the wave passes through the snowpack nearly unimpeded, without any scattering/reflection from the snowpack particles. For a shallow and dry snow cover with the SWE less than 20 cm at C-band (5.3 GHz, 5.6 cm), there is negligible volume scattering because the snow volume acts as a transparent medium for microwave at these wavelengths (Bernier 1987). For the wet snow, the compactness in the snowpack increases, which upsurges the effective snow-grain size and thickness of the snowpack (Riche, Montagnat, and Schneebeli 2013; Leinss et al. 2016).

The temporal changes in the dielectric properties of the snowpack are observed due to the variation in temperatures. The increase in snowpack wetness increases the dielectric constant of the snowpack, which also reduces the refracted energy of the microwave in the snowpack volume. Hence, the snowpack no longer remains transparent for the microwaves even for the longer wavelengths. In this case, the most significant backscatter contribution is from the air–snow interface and the snowpack volume (Nagler 1996). The effective surface roughness and the propagation path traveled by the electromagnetic waves incident at the lower angles increase, resulting in the low backscatter. Further, the electromagnetic waves at low incident angles experience more layover and shadow effects. Therefore, microwave datasets acquired at higher incidence angles are preferred for

the snow-related studies in high mountain regions (Thakur et al. 2012).

3.2.2 Polarimetric and interferometric properties and frequency response of snowpack

In general, the radar signal propagation in the snowpack is considered under two layers, the first layer being the air medium and the second being the snowpack volume, as shown in Figure 4 modified after Varade, Maurya, et al. (2020a). Within this geometry, the radar signal interacts initially with the snowpack surface at the air–snow interface, then in the snowpack volume (assuming this to be a single layer representative of the effective geophysical properties of the various layers of the snowpack), and finally at the snow–ground interface depending upon the properties of the snowpack (Ulaby, Moore, and Fung 1981). Further, the penetration of the radar signal within the snowpack is also dependent upon the incident frequency, as discussed earlier. Figure 4 shows the interaction of the radar signal with the snowpack of depth d_s , where the interferometric phase is ϕ , the line of sight displacement δd . The range difference is represented as $\Delta R = \Delta R_{sf} - (\Delta R_{sa} + \Delta R_{sg})$, where for a coherent pixel, ΔR_{sf} is the snow free range, ΔR_{sa} is the snow–air interface, and ΔR_{sg} is the range from the snow–ground interface. In Figure 4,

the refraction of the radar wave is governed by Snell's law, where θ_i and θ_r represent the angles of incidence and refraction, respectively. The fundamental processes of dominant scattering associated with the two-layer snowpack model in the context of dry and wet snow have already been discussed in the previous section. In the following paragraphs, we will discuss the polarimetric behavior of the microwave backscatter corresponding to the snowpack.

As compared to single-channel radar, the information retrievable from a polarimetric radar for a target surface increases proportionally to the number and type of channels (Cloude 2010; Pottier and Lee 2009). Typically, the observed backscattering from the co-polarized channels is higher compared to the cross-polarized channels, and maximum backscattering is in the HH polarization channel. These variations in the backscatter are typically due to the alignment of the snowpack crystals, which are usually horizontally aligned (Yueh et al. 2009). In the snow-covered areas, the average increase in the backscatter response of about 10 dB is observed for co-polarized HH and VV channels. A significantly strong backscatter response from the cross-polarization channel HV is observed in the snow cover areas due to the multiple scattering between the densely packed snow grain particles (Tse et al. 2007). Also, the HH/VV backscatter

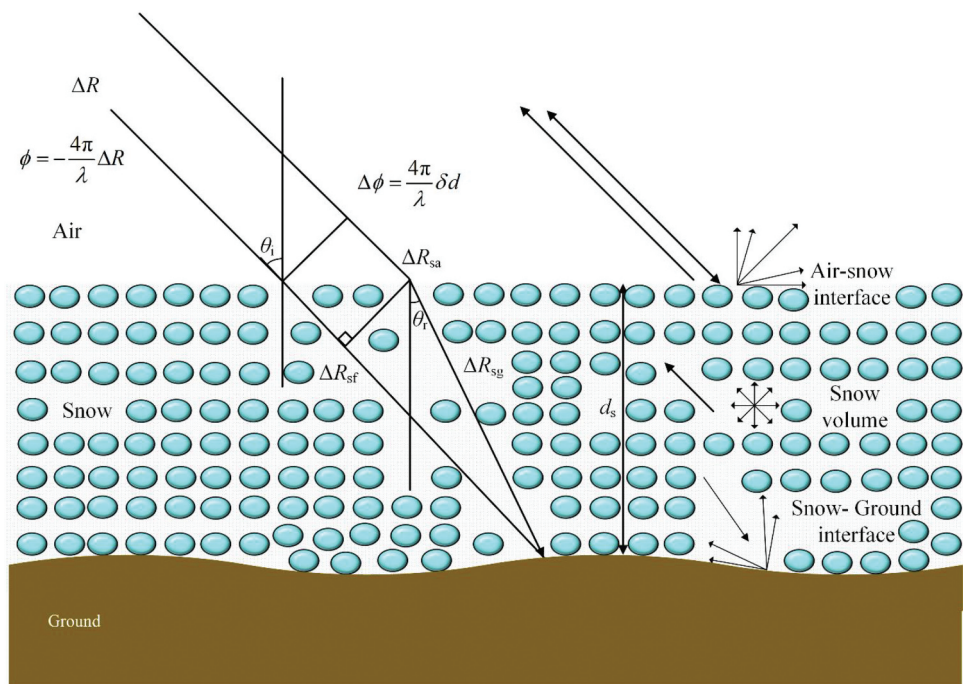


Figure 4. Propagation of microwave through the snowpack: A polarimetric and interferometric scenario (modified after (Varade et al. 2020b)).

ratio is more susceptible to the presence of volume scattering from the vegetation having more horizontally aligned tree structures, leaves, twigs, or branches over snow (Yueh et al. 2009). Other scattering mechanism with which HH/VV backscatter response is sensitive is the double-bounce scattering mechanism by ground and vegetation (Yueh et al. 2009). The transmitted microwave from the sensor is bounced off from the snow-ground interface and is scattered by the vegetation toward the direction of radar. Since the Fresnel reflection coefficient for horizontal polarization (R_h) for ground (dielectric) surfaces is larger than that of the vertical polarization (R_v), resulting in stronger HH backscatter response than in VV backscatter response in double-bounce scattering mechanism (Yueh et al. 2009).

In the vegetated areas, the temporal changes in cross-polarized backscatter response are less compared to the co-polarized backscatter response. Considering the relative volume scattering contributions from snow and vegetation, the dual polarimetric cross and co-polarized backscatter responses can be jointly utilized in separating forest areas from other regions with sparse and short vegetation covers. The ratio of cross-polarized and co-polarized backscatter responses provides the capabilities for differentiating the scattering from snow and vegetation (Yueh, Cline, and Elder 2008). In the snow-covered areas, a higher HV backscatter response is experienced compared to VV backscatter. Similarly, a high HV/VV backscatter response is observed from the high ice crust near the surface because of high HV backscatter contribution compared to VV backscatter response (Yueh et al. 2009).

The polarimetric radar backscatter in C band and X band operating frequencies show similar signatures for the wet snow (Shi and Dozier 1995), but the C-band polarimetric radar backscatter in the VH polarization channel and the X-band backscatter in the VV polarization channel provide improved separability of the dry and wet snow. This capability is due to the dominant scattering from the snow-ground interface for the dry snow at C-band and the volume scattering from the snowpack volume at the X-band (Nagler, Rott, and Glendinning 2000). But when the snowmelt begins, the dominant scattering shifts to volume scattering from the top few centimeters of the snowpack in the C-band and surface scattering at the air-snow interface in the X-band, respectively, due to the

increase in the dielectric constant of the medium. As the snowmelt initiates, the consolidation of the snow particles increases the effective size of the snow grain particles. The altered snow grain size is usually similar to the X-band wavelength. In general, the overall backscattering from the snowpack decreases quantitatively when the snow melts (Matzler et al. 1997).

Due to the dynamic nature of snow, the snowpack as a medium behaves incoherently. Yet, interferometric techniques provide useful information on the depth and the water equivalence of the snowpack. As compared to the conventional deformation studies carried out using radar interferometry, in the case of dry snowpack, the effect of the refraction at the air-snow boundary on the differential phase $\Delta\phi$ has to be considered. Here, the $\Delta\phi$ depends upon both the line of sight displacement δd and the shift in the phase due to refraction. The radar range for the snow-covered scene (ΔR_s) comprises components corresponding to path lengths for the refraction at the air-snow interface (ΔR_{sa}) and the snow-ground interface (ΔR_{sg}), as shown in Figure 4. The differences in the radar range for snow-free (ΔR_{sf}) and snow-covered conditions are given as $\Delta R = \Delta R_{sf} - (\Delta R_{sa} + \Delta R_{sg})$. Thus, the corresponding line of displacement that is related to the depth of the snowpack is defined as δd and $(\cos\theta_i - \{\varepsilon_s - \sin^2\theta_i\}^{1/2})$ (Guneriusson et al. 2001). The permittivity of snow ε_s in this formulation could be determined using empirical models for snow density as discussed earlier.

3.2.3 Passive microwave properties of the snowpack

The snowpack microwave emissions are attributed to that from the snowpack volume and the underlying ground surface. In the snowpack volume, the scattering effects cause a redistribution of the upwelling radiation corresponding to the snow thickness and snow microstructure. The redistribution of the upwelling radiation is generally modeled using the Mie scattering theory, which accounts for the snow particle size (Chang, Foster, and Hall 1987). In general, the individual particles are not spherical. However, considering the ensemble scattering properties, the particles are defined as spherical. Typically, the scattering effects are dominant when the snow particle size is comparable to the wavelength < 1 cm. In dry snow, these scattering effects are dominant, particularly at higher frequencies, such as around 37 GHz. At relatively lower frequencies around 10 GHz, the scattering

effects are lesser (Chang et al. 1976). Further, the absorption phenomena are dominant when the wavelength is much larger than the snow particle size, usually >5 cm. In this case, the brightness temperature of the snowpack is nearly similar to that of the physical temperature of the snowpack (Chang, Foster, and Hall 1987). The presence of LWC in the snowpack significantly affects the brightness temperature due to the increase in the microwave emissivity of the snowpack. In contrast to dry snow, wet snow has a higher dielectric constant, which causes a reduction in contrast with respect to the ground in terms of the brightness temperature (Chang et al. 1976).

4. Qualitative remote sensing of snow

4.1. Snow cover mapping

The spatio-temporal variability of the snow extent significantly influences the attributes of several climatic variables. Subsequently, information regarding the spatial and temporal extent of snow cover distribution is a significant input in climate models and additionally for hydrological forecasts. While conventional methods are suitable for mapping snow cover in alpine regions, several issues are observed in the application of remote sensing data and techniques for the same. Although snow is extremely bright in the visible wavelengths, it may appear relatively darker when present in shadows or in forested areas or when contaminated resulting in MI-classification of snow-covered pixels (Nolin, Dozier, and Mertes 1993). The snow cover mapping in the alpine regions is also affected by the atmospheric effects occurring due to the variations in the elevation and corresponding atmospheric composition. These effects are generally not easily removed during the atmospheric correction (Vanonckelen, Lhermitte, and Van Rompaey 2013). The all-weather capability of active microwave does enable continuous discrimination of snow from most surfaces, and they are less suitable for the discrimination of snow and glacier ice (Notarnicola et al. 2013). Typically, it is observed that microwave sensors underestimate the snow cover as compared to the optical sensors. Additionally, the extent of snow cover is usually sensitive to the microwave frequency (Shi and Dozier 1997). A bibliographical review of the various

methods used for the mapping of snow cover is detailed in the following subsections.

4.1.1 Methods based on multispectral and hyperspectral remote sensing techniques

Snow exhibits high reflectance in the visible spectrum (400–500 nm) and low reflectance in the short-wave infrared (SWIR; 1000–2500 nm) regions (Hall, Riggs, and Salomonson 1995). These properties are utilized in the NDSI, which is commonly used for the identification of snow in multispectral data (Hall, Riggs, and Salomonson 1995; Hall, Frei, and Dery 2014). The NDSI is effectively utilized for snow cover mapping and accurate delineation of the snow cover boundaries using the visible bands of the satellite imagery. However, the effects of shadows and the presence of boreal forests hinder the accuracy of snow cover estimation (Hall et al. 1998). Subsequently, this limitation was eliminated using the S3 index proposed by Saito and Yamazaki (1999), which was capable of determining snow-covered pixels mixed with vegetation.

The snow and ice products from the Moderate Resolution Imaging Spectroradiometer (MODIS) sensor available at various spatial and temporal resolutions have been efficiently used for snow cover monitoring. The snow products derived from MODIS data are available at a spatial resolution of 500 m and 1 km, with a 2330 km swath cover map along with a daily global product of fractional snow cover (FSC) climate modeling grid (CMG) map generated at 0.05-degree resolution (Zhang et al. 2003). The Landsat-8 Operational Land Imager (OLI) band 6 (1.57–1.65 μm) is efficiently used for discriminating between clouds and snow (Dozier and Painter 2004). In Ostrem, Haakensen, and Eriksson (1981), an empirical approach was developed for the measurement of remaining snow cover and to predict the corresponding snowmelt runoff volume for utilizing the NOAA and TIROS datasets of various high mountain basins of Norway.

The spatial resolution of the remotely sensed data plays a vital role in achieving precise snow cover area maps (Rango 1993). Kulkarni et al. (2006) investigated the NDSI values for a wide range of snow types using the AWiFS sensor data. Da Ronco and De Michele (2014) investigated the effect of cloud cover on MODIS snow mapping products in Po River basin in Italy. Sharma, Tateishi, and Hara (2016) developed

a new water-resistant snow index for snow cover detection and mapping on a global scale. Tekeli, Sönmez, and Erdi (2016) proposed a statistical methodology for generating satellite-derived probabilistic snow cover maps in order to define the temporal and spatial variability of snow cover in the long term. Lee et al. (2017) developed a spectral pattern recognition-based approach for snow cover detection using MODIS datasets. Wang et al. (2018) introduced a multi-index technique-based new algorithm for snow cover mapping in complex mountainous, forested environments. Masson et al. (2018) worked on the assessment of existing methodologies for the retrieval of snow cover fraction from MODIS datasets. Berman et al. (2018) demonstrated a method for deriving 30-m daily SCA product over large mountainous and forested regions using Dynamic Time Warping (DTW) algorithm, exploiting the daily revisit MODIS product. Kuter, Akyurek, and Weber (2018) demonstrated a multivariate adaptive regression-based approach for retrieving the fractional snow-covered areas.

Varade, Sure, and Dikshit (2019) proposed a simple feature selection-based approach to develop SI (Snow Index) from the hyperspectral data using the best band in green spectrum and SWIR spectrum, specifically 196 Hyperion band reflectance after atmospheric correction for the Dhundi area in the lower Indian Himalayas. Poussin et al. (2019) developed Earth Observations Data Cubes (EODC) using Landsat-8 images for monitoring snow cover evolution in the Italian Alps. Singh et al. (2019) proposed an algorithm for the detection of seasonal snow cover variations using fuzzy classification integrated with change vector analysis (CVA) for North Indian Himalayan region. This study also analyzed the temporal variability of the snow cover in the region. Hou et al. (2019) used Machine Learning (ML) based non-local spatio-temporal filtering for formulating the MODIS Fractional Snow Cover Products. A thresholding-based unsupervised adaptive Gaussian mixture Model Integration algorithm was developed for snow cover mapping in mountainous areas (Zhang et al. 2020).

Rittger et al. (2020) proposed a vegetation correction-based approach for increasing the accuracies of snow mapping in the forested areas. During the snow cover mapping in the forested areas, vegetation canopies cause interferences, and ground surfaces are not

visible to the satellites resulting in uncertainty in the snow cover products. High-resolution SCA maps were developed from Sentinel-2 and Landsat-8 imagery as part of the Theia collection containing four classes: snow, no snow, cloud, and no data (Gascoin et al. 2019). Gascoin et al. (2020) evaluated a simple empirical function to estimate fractional snow cover (FSC) using Sentinel-2 datasets using NDSI. Table 1 summarizes some of the methods developed in the literature for the mapping of snow cover based on optical remote sensing data. For the mapping of SCA, Baba et al. (2020) evaluated the standard thresholding-based method with a modified normalized differenced snow index and proposed a machine learning-based method accounting for the advantages of supervised and unsupervised classification.

4.1.2 Methods based on active microwave remote sensing techniques

Microwave remote sensing techniques have been extensively utilized for snow cover mapping (Dozier 1989; Manickam et al. 2016; Nagler, Rott, and Glendinning 2000; Ulaby et al. 2014; Ulaby et al. 1977; Varade et al. 2020c). With the launch of SeaSat in 1978, there was an initiation of the era of utilizing the spaceborne SAR sensor datasets for the snow cover monitoring (Pepe et al. 2005). Shi, Hensley, and Dozier (2000) analyzed the multi-frequency L band and C band SAR datasets for snow mapping in Oetztal Alps region of Austria. The retrieved results were validated using the Landsat TM datasets and showed a high accuracy during wet snow-covered areas using the co-polarization channels. Shi and Dozier (1997) developed a method using the SIR-C/X-SAR data to classify the seasonal snow cover area in the Mammoth Mountain ranges of Sierra Nevada using the classification approaches based on intensity measurements, polarization properties, and frequency ratios. High classification accuracy of 79% was achieved in this study for the classification of the seasonal snow cover area.

Enhanced snow-cover mapping accuracy was obtained by incorporating interferometric coherence in addition to SAR backscatter information (Strozzi, Wegmüller, and Matzler 1999). Ferro-Famil et al. (1999) analyzed the variation in the L- and C-band polarimetric descriptor parameters like entropy, alpha angle, and anisotropy due to seasonal variations in the snow-covered area using airborne radar

**Table 1.** Methods of snow cover mapping based on multispectral and hyperspectral remote sensing techniques.

S. No.	In-Text citation	Deliverable, Sensor, resolution	Approach/Formulae	Comments
1.	Hall, Riggs, and Salomonson (1995)	Daily/Weekly Snow Cover at Global scale, MODIS, 500 m	Refined SNOMAP prototype algorithm using TM data to enable automated mapping using MODIS data.	Classification algorithms provided more consistent results compared to supervised classification techniques
2.	Saito and Yamazaki (1999)	SCA	Spectral analysis to distinguish the snow cover and vegetation	Characterization of vegetation and snow cover using spectral reflectance
3.	Dozier and Painter (2004)	SCA, Landsat TM, 30 m	Multispectral and hyperspectral remote sensing approaches for snow properties estimation	Analysis of the sub-pixel variability of the snow-covered areas along with the albedo
4.	Sharma, Tateishi, and Hara (2016)	SCA, MODIS, 500 m	Water-resistant Snow Index (WSI) for snow cover mapping excluding the water bodies.	Capable of exhibiting significant contrast between snow cover and water bodies.
5.	Tekeli, Sonmez, and Erdi (2016)	SCA, IMS snow product	Statistical approach using Interactive Multi Sensor Snow and Ice Mapping System (IMS)	Characterization of the temporal and spatial variability of the snow cover based on long-term IMS snow cover maps.
6.	Lee et al. (2017)	SCA,	Spectral pattern recognition-based snow cover detection	Algorithm based on dynamic time warping (DTW) using MODIS datasets
7.	Wang et al. (2018)	SCA, MODIS, 500 m	Multi-indices-based technique for snow cover mapping	Combination of NDSI, the normalized difference forest snow index, and the normalized difference vegetation index, and decision rules for snow mapping in forested areas.
8.	Varade, Maurya, and Dikshit (2019a)	NDSI, SCA, MODIS, 500 m	Spectrum-based band selection scheme to determine best visible and SWIR bands for NDSI	A generic approach for NDSI estimation using hyperspectral data
9.	Hou et al. (2019)	Hyperion, 30 m	Implementation of non-local spatio-temporal filtering based on ML	The approach for Gap-Filling of MODIS Fractional Snow Cover Products due to Cloud obscuration
10.	Gascoin et al. (2019)	Fractional Snow Cover, MODIS, 500 m	Multi-stage processing algorithm accounting for snow detection, snow line elevation, and cloud mask processing	Accurate detection of SCA and snow free area, particularly compared with Sen2cor algorithm
11.	Zhang et al. (2020)	SCA, FY-4A satellite data, 500 m	Unsupervised Gaussian mixture model (GMM) algorithm for snow cover detection.	Accurate snow detection algorithm in mountainous terrain
12.	Rittger et al. (2020)	SCA, MODIS, 500 m	MODSCAG algorithm for linear spectral mixture analysis for determining subpixel coverage	Approach incorporating Canopy Adjustment and Improved Cloud Detection
13.	Baba et al. (2020)	SCA, VENus, Sentinel-2 5 m, 20 m	Standard thresholding and classification based approaches using SVM	Results evaluated using Theia snow collection products are subject to the classification algorithm used

Table 2. Methods of snow cover characterization based on microwave remote sensing techniques.

S. No.	Methods	SCA/Snow Type, Sensor, resolution	Approach/Formulae	Comments
1.	Shi and Dozier (1997)	SCA, SIR-C/X-SAR, 30 m	Coherence and backscattering measurements	Analysis of interferometric coherence measurements
2.	Holden, Solberg, and Solberg (1998)	Wet snow cover, Airborne EMISAR, 5 m	Clustering-based supervised classification approach for wet snow mapping using multi-polarization datasets	Dual frequency C- and L-band SAR data used
3.	Strozzi, Wegmüller, and Matzler (1999)	Wet snow cover, ERS, 30 m	H-A-E classification and polarimetric change parameterization	Interferometric SAR datasets of ERS-1 for mapping snow wetness
4.	Ferro-Famil et al. (1999)	dry SCA, SIR-C SAR, 30 m	Classification approaches for discriminating dry from wet snow with and without using a DEM	Evaluation of Full polarimetric SAR for classifying Dry snow cover.
5.	Shi, Hensley, and Dozier (2000)	SCA, SIR-C SAR, 30 m	Classification approaches for discriminating dry from wet snow with and without using a DEM	Incorporation of Digital Elevation Model information for mapping seasonal snow
6.	Nagler and Rott (2000)	Wet snow, ERS-1, 30 m	Analyzing backscatter variation in multi-temporal SAR Datasets for mapping wet snow cover	The effect of the different look angles on wet snow mapping is analyzed in the study
7.	Mahnés and Gunnerusen (2002)	Dry/Wet Snow Area, RADARSAT-1, 25 m	Improved version of Nagler SCA-algorithm (Nagler and Rott 2000)	A sub-pixel method for snow classification is suggested
8.	Pepe et al. (2005)	SCA, MERIS, 260 × 290 m, AATSR, 1000 × 1000 m	Based on the combined use of ENVISAT optical data and topographic information	A multisource classification scheme is developed here.
9.	Rao, Venkataraman, and Singh (2006)	SCA, ENVISAT-1 ASAR, 30 m	Backscatter based thresholding approach for snow cover area mapping	The value of threshold was area dependent
10.	Nagler et al. (2008)	Wet snow ENVISAT-1 ASAR, MODIS 30 m and 500 m	Assimilation of meteorological and remote sensing data	A semi-distributed model is used during short-term runoff forecasting
11.	Singh et al. (2008)	SCA, ALOS-PALSAR-1, 30 m	H/A/Alpha Polarimetric Decomposition and Complex Wishart Distribution based approach for Snow Cover Monitoring	Study relates size of the Lee filter window for speckle reduction and classification accuracy
12.	Singh et al. (2014)	SCA, ALOS-PALSAR-2, 6 m	Snow-covered area estimation applying scattering mechanism models	Assessment of fully polarimetric L-band data for snow and non-snow area classifications
13.	Usami et al. (2016)	Wet snow Area, ALOS-2 PALSAR-2, 6 m	Simplified integral equation model (IEM) based approach for wet snow mapping	Degree of polarization (DOP) parameter utilization for estimating effective snow wetness, by considering incident angle information
14.	Nagler et al. (2016)	Snow Melt area Sentinel-1, 5 m × S20m	Weighted integration of bi-temporal backscatter ratio (snow covered/snow-free) in VV and VH channels	A change detection method for snowmelt classification using multi-temporal dual-polarized SAR datasets
15.	Muhuri, Ratha, and Bhattacharya (2017)	SCA, RADARSAT-2, 3 m	Incorporating co-polarized (HH-VV) correlation coefficient and the total scattering power for Seasonal Snow Cover Change Detection	Multi-temporal analysis of the polarimetric variables for snow cover change detection
16.	He et al. (2017)	Dry/Wet Snow RADARSAT-2 and GF-1 3 m and 16 m	Two-step method for dry and wet snow cover identification using interferometric coherence and backscattering coefficient	The proposed method highly depends on prior knowledge obtained from in situ measurements
17.	Muhuri et al. (2018)	SCA, RADARSAT-2, 3 m	Polarization Fraction Variation based Snow Cover Mapping Approach	Mapping of snow cover using RADARSAT-2 C-Band
18.	De et al. (2018)	SCA, RADARSAT-2, 3 m	Neural Network based approach for snow cover mapping	Full-Polarimetric SAR Data Utilizing of multi-basis Pointcare sphere parameters for snow cover mapping
19.	Snapir et al. (2019)	Dry/Wet Snow Sentinel-1 and MODIS 10 m and 500 m	fusion of MODIS fractional snow cover and Sentinel-1 wet snow mask for estimating wet and dry snow	Utilizing auto-encoder network. Sentinel-1 highlighting the snow melt phase with the decrease in snow depth
20.	Varade, Dikshit, and Manickam (2019)	Dry/wet snow, Sentinel-1 and Sentinel-2, 20 m	extension of Nagler et al. 2016 for wet snow mapping. The dry snow is determined from the SCA using the multispectral data	Simple approach, issues related to sensor synergy, inapplicability during cloud cover
21.	Varade et al. (2020c)	SCA, ALOS-PALSAR-2, RADARSAT-2, 20 m (resampled)	Incorporates the fully polarimetry entropy and anisotropy for a radar index "Radar Snow Fraction" for snow detection	Relatively less sensitivity to dry/wet snow, forest cover, and look direction as compared to other parameters
22.	Karbou et al. (2021)	Wet snow, Sentinel-1 and Sentinel-2, 20 m	Follows the approach by (Nagler et al. 2016) and investigates the influence of terrain parameters on snow distribution	Investigations revealed that differences in snow cover exists for Sentinel-1 (underestimated) and Sentinel-2 for forests and glaciers For monitoring wet snow over French Alps, ascending/descending Sentinel-1 passes are complimentary

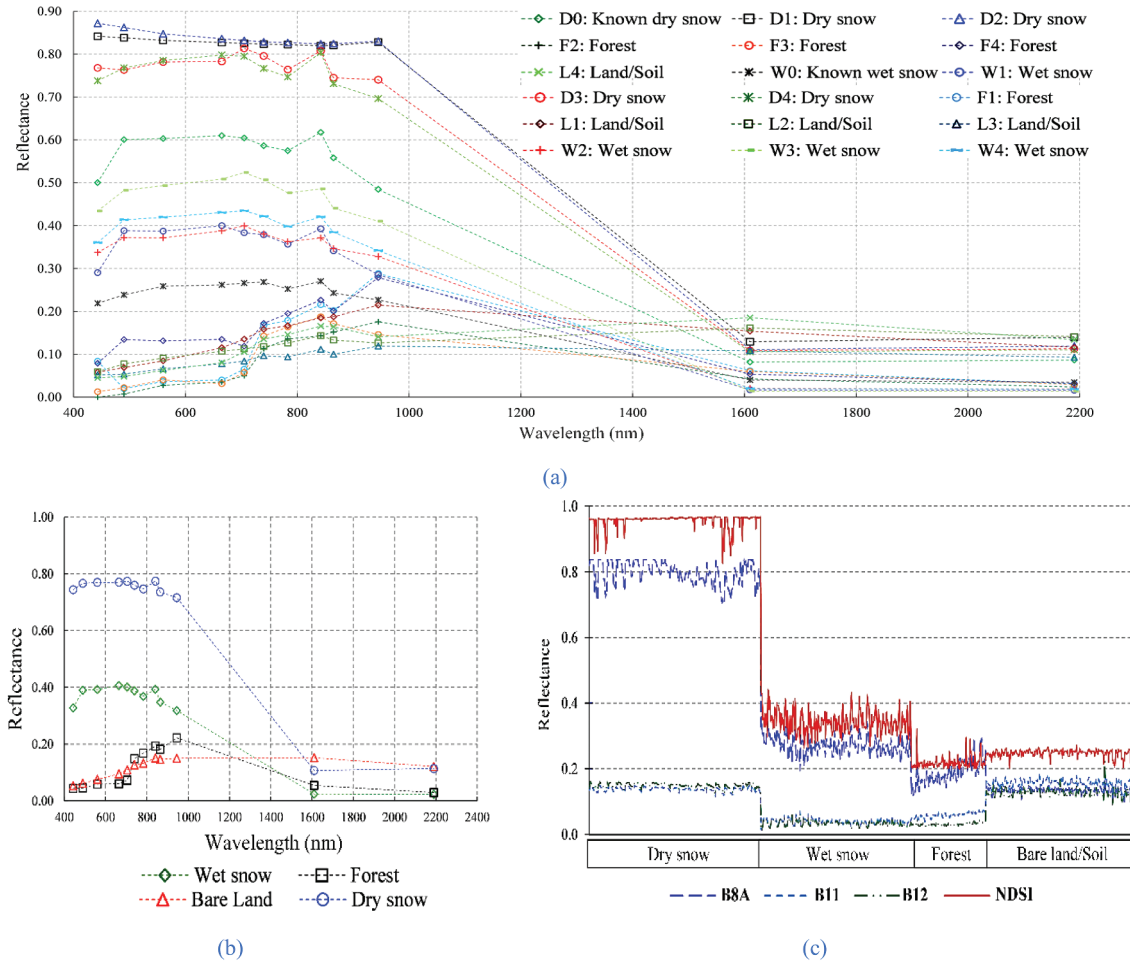


Figure 5. Spectral reflectance in the different wavelengths of Sentinel-2 bands (modified after (Varade and Dikshit 2018)) (a) for various samples corresponding to different land cover. (b) Mean spectral response from (a), (c) Comparison of NDSI and the NIR (B8A) and SWIR (B11 and B12) reflectance for selected samples.

polarimetry. Singh et al. (2008) used H/A/Alpha decomposition, Wishart classifier, and polarization fractional value for snow classification using L-band full polarimetric ALOS-PALSAR datasets. Thakur et al. (2013) proposed an approach for snow cover area mapping using the C-band Radarsat-2 datasets in the Northwest Himalayan regions. The proposed approach used the ratio image of wet snow and dry snow, with the variable threshold for snow cover area mapping. Techniques based on bi-temporal fully polarimetric datasets have been shown to be more precise for snow cover mapping.

Muhuri, Ratha, and Bhattacharya (2017) suggested an approach for snow cover mapping that utilized Touzi eigenvalue-eigenvector-based decomposition parameters i.e. the scattering helicities (τ_m), the scattering magnitude (α_s) and Entropy (H) using ALOS-2 datasets in the Himalayan region. The seasonal variation of these parameters was used as an indicator for snow

cover variation analysis. Muhuri et al. (2018) developed a method for seasonal snow cover change detection using the C-band polarimetric SAR RADARSAT-2 datasets for the Manali region of India. This approach used the index ratio of the co-polarized correlation coefficient (HH-VV) and the total scattering power for efficient snow cover change characterization as a means of snow cover mapping. However, these methods require multi-temporal fully polarimetric datasets, which are typically very expensive and are thus cost-inefficient. De et al. (2018) proposed a novel framework for snow cover mapping with multi-basis Poincaré sphere parameters auto-encoder network-based algorithm. Evidently, such methods are supervised, requiring high confidence reference data for training the auto-encoder network and additionally also involve higher computational complexity.

Considering the limitations of the aforementioned methods, simple approaches that utilize a minimum

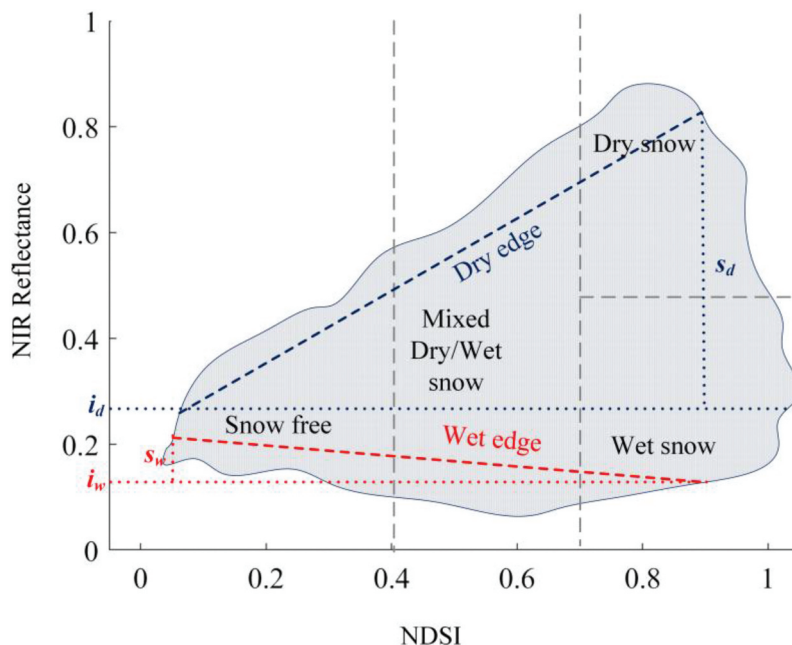


Figure 6. The triangle method based on the NIR-NDSI feature space for the determination of snow LWC (modified after (Varade and Dikshit 2018)).

number of parameters are usually preferred for snow cover mapping (Muhuri et al. 2018; Nagler, Rott, and Glendinning 2000; Rao, Venkataraman, and Singh 2006; Singh et al. 2014; Varade et al. 2020c). Singh et al. (2014) examined the capabilities of L-band fully polarimetric datasets for snow and non-snow area classifications. The study used various parameters like backscattering coefficients, co-polarized and cross-polarized backscatter ratio, and polarization fraction (PF) value for discriminating snow-covered and non-snow-covered areas. This study demonstrated the application of the radar snow index (RSI) developed using the PF and the third eigenvalue of the coherency matrix. Varade et al. (2020c) proposed a novel radar index – radar snow fraction (RSF) for snow cover mapping using fully polarimetric parameters like entropy (H) and anisotropy (A) with a sigmoidal activation function. They examined the RSF for multiple datasets in the Indian Himalayas using ALOS-2/PALSAR-2 (L-band) and RADARSAT-2 (C-Band) datasets and observed that the RSF outperformed the conventional RSI. This study also revealed the dependency of the other parameters over the type of snow, presence of forests, and the orientation of the mountain slopes with respect to the snow identification.

4.1.3 Methods based on passive microwave remote sensing data

In section 3.2.3, we discussed the contrast in brightness temperature for snow and the ground surface. This approach is utilized in the determination of the snow

cover extent (Kunzi, Patil, and Rott 1982). Kunzi, Patil, and Rott (1982) mapped the snow cover extent using the spectral gradient method for shallow snow. The snow cover was determined using the difference of brightness temperatures at 18 GHz and 37 GHz based on thresholds of 3.8 K, such that the differenced values greater than this threshold determine snow. Several studies based on SWE estimation also accounted for snow cover extent determination by including different thresholds (Chang et al. 1976; Chang, Foster, and Hall 1987). Vertically polarized microwave data with the spectral difference approach has been observed to be useful for differentiating snow and snow-free conditions (Hallikainen 1989). Nagler (1991) utilized the 89 GHz band of SSM/I sensor by incorporating an additional spectral difference between the 37 GHz and the 89 GHz channels along with the conventional 18 GHz and the 37 GHz channels for the determination of snow cover extent. The addition of the 89 GHz component rendered this approach to be more sensitive to thin snow. An investigation of the spectral emissivity signatures of various surfaces was carried out by Matzler to distinguish snow from snow-free surfaces in various areas (Matzler 1994).

4.2 Snow cover characterization

There are several ways of characterizing snow either based on the amount of the LWC in the snow, the snow grain size or shape, the density, other parameters like the permittivity, or based on the spectral

reflectance, which itself depends upon the properties mentioned above. Thus, the characterization could be regarded in terms of the qualitative observations of these properties or the quantitative properties, as discussed in the next section.

4.2.1. Snow classification

The qualitative spatio-temporal variability of SGP is speculative at best since it is not possible to validate this comprehensively. This follows from the fact that the volume of field measurements required for such a purpose is simply not feasible practically. Thus, the classification of snow based on these properties is one of the methods that could provide significant insights regarding the spatio-temporal variability of SGP. Fully polarimetric SAR data can retrieve precise information on these parameters and is thus, a potential candidate for training the classifiers and validating the classification results. However, a precise validation is possible only for small regions, as the spatial coverage of fully polarimetric SAR data is significantly smaller as compared to the available multispectral data or the hyperspectral data. Another important aspect to note in this process is the tolerable duration between the passes of the optical remote sensing data and the fully polarimetric SAR data. Subsequently, few studies on the classification of snow exist in the literature (He et al. 2017; Muhuri, Ratha, and Bhattacharya 2017; Nagler et al. 2008; Varade et al. 2020c). The classification of the snow is carried out either based on the reflectance, including classes such as high or low reflectance snow, or based on the percentage of LWC. In the case of the former, the reference data is prepared based on experience and visual interpretation of the scene (Varade et al. 2018; D. Varade, Maurya, et al. 2019), while in the case of the latter, the reference data is prepared based on modeled products from fully polarimetric SAR data (D. Varade, Maurya et al. 2019).

4.2.2. Dry/wet snow determination

The spatial variability in terms of the dry/wet characterization is significant for the understanding of phenomena such as avalanche. However, new dry snow is nearly transparent for millimeter-wave signals and is thus difficult to identify (Ulaby et al. 2014). In contrast, the backscatter from a wet snowpack is significantly sensitive to the LWC in the snowpack, rendering wet snow mapping to be feasible (Nagler, Rott, and

Glendinning 2000). Further, from the perspective of optical remote sensing, the NIR reflectance also shows sensitivity to the LWC in the snow surface layer. Gupta, Haritashya, and Singh (2005) showed that the NIR reflectance is capable of differentiating wet and dry snow. However, based on the inferences of Dozier and Green (Dozier et al. 2009), the wet snow, in this case, may be mistaken for refrost snow. This observation also holds for the triangle method discussed in section 5.1.1 proposed by Varade et al. (2018) for estimating snow LWC. However, since multispectral passes in the lower Indian Himalayas are typically scheduled in the late mornings, the presence of liquid water on snow surfaces in sunny days is not questionable. Nevertheless, methods based on microwave remote sensing data alleviate this issue due to their penetrability and direct influence on backscatter from the dielectric properties of the snowpack.

Microwave backscattering-based multi-frequency analysis was conducted for this wet snow mapping using L band and C band SAR datasets (Holden, Solberg, and Solberg 1998). Nagler, Rott, and Glendinning (2000) proposed a single-channel backscatter ratio method between snow-free and snow-covered scenes for the mapping of wet snow. A model-based approach was developed using an improved Nagler SCA algorithm for snow cover area estimation using SAR datasets in the Himalayan region and mountainous regions of Norway (Malnes and Guneriussen 2002; Rao, Venkataraman, and Singh 2006). A robust algorithm for the snow wetness mapping was developed using ENVISAT datasets of the Himalayan region (Singh et al. 2006). The study incorporated Physical Optics Model (POM) based inversion model on radar backscattering for the estimation of snow dielectric constant and snow wetness mapping (Singh et al. 2006). Further, Storvold and Malnes (2004) proposed an improved wet and dry snow cover classification approach using ENVISAT ASAR wide swath datasets by incorporating the air temperature data from the Norwegian Meteorological Station Network to create high-resolution surface air temperature maps. The results from this approach were later validated using the optical sensor datasets and the high accuracy field measurements.

Luoju et al. (2007) proposed an improved approach for monitoring wet snow cover areas in the boreal forest regions. Luoju et al. (2007) demonstrated a two-step approach for mapping wet snow

cover over Boreal forest in Finland using ERS-2 multi-temporal datasets. A relatively lower backscatter intensity was observed in the wet snow areas compared to the snow-free regions (Nagler et al. 2008). Further, Nagler et al. (2016) extended this method for the dual polarimetric systems by including a weighting scheme for the ratios in the co-polarization and the cross-polarization channels. He et al. (2017) investigated 36 fully polarimetric parameters from RADARSAT-2 data for the mapping of wet and dry snow. They inferred that the Pauli volume scattering, the third eigenvalue of the coherency matrix, and the volume scattering of the Yamaguchi four-component decomposition model showed good mapping results for wet and dry snow. However, the performance of this method was constrained by the quality of the reference data used for the evaluation in this study. The assessment of the parameters in this study was carried out using the support vector machines with the reference data determined from the method by Nagler and Rott (Nagler, Rott, and Glendinning 2000), which uses only a single co-polarized channel.

Varade, Sure, and Dikshit (2019) used a multi-sensor approach integrating the NDSI and the dual polarimetric ratio method proposed by Nagler et al. (2016) for mapping dry and wet snow by using supervised and unsupervised methods. In this study, the modeled LWC based on the general four-component scattering power decomposition with the unitary transformation (G4U) decomposition of the coherency matrix. Snapir et al. (2019) utilized a similar approach by determining the monthly maximum wet snow maps using the dual polarimetric ratio method and the snow cover fraction using the monthly MODIS data for the identification of dry snow as the difference of these two products (Nagler, Rott, and Glendinning 2000; Varade, Dikshit, and Manickam 2019). Usami et al. (2016) proposed a method for wet snow mapping using the incidence angle information applying the supervised learning technique in a quaternion neural network. He et al. (2017) proposed a two-step process using SAR polarimetry and interferometry-based techniques using fully polarimetric SAR datasets along with optical datasets and the ground measurements for wet snow mapping and snow cover characterization.

Table 3. Various methods utilizing active microwave remote sensing data for the estimation of SGP (dielectric constant, wetness, and density).

S. No.	Methods	Estimated parameter(s), Sensor, resolution	Approach/Formulae	Comments
1.	Shi and Dozier (1995)	Wetness, SIR-C/X SAR, 30 m	Polarimetric first-order backscatter model considering both surface and volume scattering by utilizing both co-polarization channels	An active microwave remote sensing-based inversion modeling approach for snow parameters estimation.
2.	Shi and Dozier (2000a)	Density, dielectric constant, SIR-C's L-Band SAR, 30 m	Polarimetric first-order backscatter model for estimating dry snow density, the dielectric constant, and the roughness of the soil layer beneath the snowpack using co-polarization channels	A root mean square error of 0.042 g/cm ³ for the snow density estimates with respect to in-situ measurements.
3.	Singh et al. (2006)	Wetness, ENVISAT-ASAR, 30 m	Physical Optics Model (POM) based inversion model for estimation of snow dielectric constant and snow wetness using radar backscattering coefficients	Representing snow surface backscattering as function of permittivity of snow for estimating snow wetness.
4.	Bhattacharya et al. (2014)	Wetness, TerraSAR-X, 3 m	IEM-based scattering model with Rayleigh scattering assumption	Polarimetric Scattering Angle (α_1) used as dominant surface scattering parameter, random particle scattering estimated using particle anisotropy (A). G4U decomposed T_3 matrix components are used to derive the Fresnel coefficients.
5.	Surendar et al. (2015)	Density, Radarsat-2, 3 m	G4U-based generalized volume parameter for estimating snowpack dielectric constant using the Fresnel transmission coefficients.	G4U decomposed T_3 matrix components are used to derive the Fresnel coefficients.
6.	Manickam et al. (2016)	Surface dielectric constant, RADARSAT-2, 3 m	Maximum surface scattering pixels are used for inversion of dielectric constant. These pixels are identified by the dominant scattering mechanism and optimal degree of polarization.	Correlation coefficient was found to be 0.95 at 95% confidence interval, RMSE of 0.20; only applicable to wet snow surface
7.	Singh et al. (2017)	Density, TerraSAR-X, 3 m	Generalized Singh-Cloude 3 component hybrid decomposition model	Fully polarimetric SAR approach for estimating snowpack density in the seasonal snow-covered region is developed.
8.	Varade et al. (2020a)	Density, dielectric constant, RADARSAT-2, 8 m	Utilizes bi-temporal fully PolSAR data for the retrieval of modified scattering matrix used for the modeling of Fresnel transmission coefficients	Relatively robust to changes in wetness and depth, for old/settled snow and dry snow, outperformed the decomposition methods for old snow
9.	Awasthi et al. (2020)	Density, RISAT-1, 3 m	IEMbased approach for modeling Fresnel coefficients for inversion of snow density based on Hybrid Polarimetric datasets used	Efficient Hybrid Polarimetry approach for Snow Density estimation using roll-invariant SAR observable parameters

Table 4. Various methods utilizing active microwave remote sensing data for the estimation of SGP (snow depth and SWE).

S. No.	Methods	Estimated parameter(s), Sensor, resolution	Approach/Formulae	Comments
1.	Shi and Dozier (2000b)	SWE, depth, SIR- C's L-Band SAR, 30 m	Semi-empirical models for characterizing snow–ground interaction terms, relationships between the ground surface backscattering components, and the snowpack extinction properties	A backscatter model for the estimation of snow grain size and snow depth in the dry snow using the C band Shuttle Imaging Radar (SIR-C) data
2.	Leinss, Parrella, and Hajnsek (2014)	depth, TerraSAR-X/ TanDEM-X, 3 m	Co-polar phase difference (CPD) between VV and HH polarizations	Time-Series CPD from TerraSAR-X and TanDEM-X were analyzed for fresh snow
3.	Li et al. (2017)	Depth and SWE, ENVISAT ASAR	Repeat pass SAR Interferometry approach for Snow Depth and SWE estimation	Theoretical method for snow depth estimation using ENVISAT ASAR IMS data.
4.	Lievens et al. (2019)	Depth, Sentinel-1, 1 km ² (resampled)	Snow depth estimation approach based on temporal changes in the Sentinel-1 backscatter polarization ratio ($\sigma^0_{vh}/\sigma^0_{vv}$) and scaled to the range of snow depth measurements at in situ sites	Snow Depth retrievals using Sentinel-1 datasets; over the entire Northern Hemisphere mountain ranges
5.	Varade et al. (2020a)	Density, dielectric constant, RADARSAT-2, 8 m	Utilizes bi-temporal fully PolSAR data for the retrieval of modified scattering matrix used for the modeling of Fresnel transmission coefficients	Relatively robust to changes in wetness and depth, for old/settled snow and dry snow, outperformed the decomposition methods for old snow
6.	Varade et al. (2020b)	Depth, Sentinel- 1, 15 m	Weighted scaled adjusted sum of bias corrected line of sight DInSAR displacements	Very high correlation compared to DInSAR displacements, lower RMSE due to scale adjustment, apriori mean depth needed from in-situ measurements
7.	Mahmoodzada, Varade, and Shimada (2020)	Depth, Sentinel- 1, 15 m	Extention of (Varade et al. 2020b), where spatially distributed permittivity is incorporated in snow phase shift correction	Investigations in peak winter and early melt seasons, sensitivity to wetness
8.	Patil, Mohanty, and Singh (2020)	Depth and SWE, Quad Pol- TerraSAR-X 3 m	PollnSAR coherence based snow depth estimation approach based on bistatic TerraSAR-X datasets	Study showcased PollnSAR Coherence correlation with SD and SWE using Full-Pol TerraSAR-X datasets
9.	Patil, Singh, and Rüdiger (2020)	Depth and SWE, Dual Pol- TerraSAR-X 3 m	Approach utilizing the relationship between Snow Depth, co-polar phase difference (CPD), and particle anisotropy for depth and SWE estimation using TerraSAR-X dual PolSAR data	A modified CPD model for SD and SWE estimation using variable snow density and anisotropy
10.	Awasthi et al. (2021)	Depth TerraSAR-X/ TanDEM-X, 3 m	PollnSAR based inversion modeling approach for snow Depth estimation using pursuit-monostatic TanDEM-X datasets in North-Western Himalayan region	Coherence Amplitude inversion based PollnSAR modeling for snow depth variability analysis

Karbou et al. (2021) analyzed the seasonal wet snow cover extent using the method proposed by Nagler et al. (2016) and investigated the influence of mountain topography on snow distribution by considering terrain parameters such as altitude, slope, and aspect. Table 2 illustrates some of the methods in the literature for the identification of SCA and wet/dry snow based on active microwave remote sensing data and or fusion of the active microwave remote sensing data with optical remote sensing data.

5. Quantitative remote sensing of snow

5.1. Methods based on optical remote sensing

5.1.1. Surface snow LWC and density

Conventionally, the usage of optical remote sensing for quantitative assessment of SGP is very limited due

to the poor penetrability of the EM wave in the visible and infrared (including thermal) spectrum. Thus, with optical remote sensing, the information on the SGP can only be retrieved for the surface layer. Varade and Dikshit (2018) proposed the triangle for the quantitative measurement of snow LWC, inspired by Sadeghi et al. (2017) and Lampkin and Yool (2004). They performed an investigation to identify the best bands of Sentinel-2 multispectral data with the highest sensitivity to the wet snow. Figure 5, modified after Varade and Dikshit (2019) shows the reflectance of various land cover based on Sentinel-2 multispectral data based on the field observations at study area in the Solang Valley, Himachal Pradesh, India. The triangle feature space comprising the NIR reflectance and the NDSI proposed by Varade and Dikshit (2019) is shown in Figure 6 with overlaid dry and wet edges whose

intercepts and slopes are used to compute the snow LWC as shown in equation (4) as:

$$w = \frac{i_d + s_d NDSI - R}{(i_d - i_w) + (s_d - s_w) NDSI} \quad (4)$$

where w is the snow LWC given in Vol. %, i and s are the intercept, and the slopes of the dry and wet edges denoted by subscripts "d" and "w," respectively, and R is the NIR reflectance of the 865 nm band of Sentinel-2 multispectral data.

Lampkin and Yool (2004) proposed the near-surface moisture index (NSMI) that models the surface moisture using visible and thermal spectra. Varade and Dikshit (2019) extended their method (Varade and Dikshit 2018) for estimating the surface density and the permittivity by incorporating state of the art empirical models in a least-squares framework. The empirical models used in Varade, Sure, and Dikshit (2019) are based on the linear mixing of the dielectric constant of the dry snow (ϵ_{ds}) with the increment in dielectric constant ($\Delta\epsilon_{ws}$) due to the introduction of LWC for the determination of the dielectric constant of the wet snow as $\epsilon_s = \epsilon_{ds} + \Delta\epsilon_{ws}$ (Denoth 1994; Tiuri et al. 1984; Kendra, Ulaby, and Sarabandi 1994). Eppanapelli et al. (2018) showed that the normalized differenced water index (NDWI) developed using the mean reflectance values in the 980 and 1310 nm can be used for modeling the snow LWC. Haq et al. (2019) utilized the artificial neural network to develop regression models for the estimation of snow LWC and density using hyperspectral data and field spectra measurements of snow comprising different levels of LWC and various densities.

5.1.2. Surface snow grain size

In practice, the conventional snow grain size index mainly provides qualitative information on the variability of the snow grain size from fine to coarse (Dozier 1989). Negi and Kokhanovsky (2011) used the asymptotic radiative transfer (ART) theory for the retrieval of snow grain size in the western Himalayas using Hyperion data. The reflectance in the 440 nm in the visible and the 1050/1240 nm in the NIR region was used to retrieve the snow grain size, which was evaluated with the field spectrometer retrieved snow grain size. Nolin and Dozier (2000) proposed an inversion technique based on a radiative transfer method that utilizes the ice absorption feature in the 1030 nm region to estimate the snow grain size. The

experiments for this method were conducted using the Airborne Visible/Infrared Imaging Spectrometer (AVIRIS) data over the eastern Sierra Nevada in California, United States. They observed the results to be robust and accurate, corresponding to the ground-based spectrometer data and grain size measurements. Painter et al. (2003) proposed an automated multiple endmember spectral mixture analysis-based approach for the estimation of snow grain size. This study was carried out using AVIRIS data for a study area in the Mammoth Mountains of California, United States. This method overestimated the grain size by 4%–7% for the investigated data.

5.1.3. Determination of snow depth using optical remote sensing

Aerial surveys using unmanned aerial systems (UAS) have found wider applications in the estimation of snow depth based on stereophotogrammetric and laser scanning techniques (Adams, Bühler, and Fromm 2018; Bühler et al. 2015; Goetz and Brenning 2019; Vander Jagt et al. 2015). Since the focus of the present review is on satellite-based remote sensing studies, a perspective of UAS for the estimation of snow depth is out of the scope here. In general, the methods in both airborne and or space-borne optical remote sensing are similar. These methods typically involve conventional approaches utilizing stereophotogrammetry and laser scanning based DEM differencing between snow-covered scenario to snow-free scenario for the estimation of snow depth. Treichler and Kääb (2017) investigated the potential of ICESat laser altimeter for the estimation of regional-scale snow depths during the winter and spring seasons and observed that the depth time series agreed well with an RMSE of <0.47 compared to the measured snow depths in the Scandinavian mountains in southern Norway.

Marti et al. (2016) investigated the potential of very high resolution (VHR) satellite stereo images for the estimation of snow depth. In their study, two triplets of 0.7 m resolution Pléiades satellite images were used for the determination of bias-corrected DEM differences, which were compared with snow probe measurements. They reported from this comparison median residuals of 0.16 m and a standard deviation of 0.58 m. Shaw et al. (2020b) extended the approach by Marti et al. (2016) by correcting and filtering the Pléiades snow depths based on a Gaussian mixture model surface classification of the

snow-free areas and utilizing a random forest model for data gap filling. In an extension of this study, Shaw et al. (2020b) compared the pixel-to-pixel grouped snow depth differences based upon topographic indices, including aspect, slope, etc. and observed that the most significant differences in snow depth and snow-covered area are linked to these parameters. Deschamps-Berger et al. (2020) further improve upon the evaluation carried out in Shaw, Shaw et al. (2020a) for the Tuolumne River basin using accurate snow depth maps derived from Airborne Snow Observatory laser-scanning measurements. Eberhard et al. (2020) performed comparative measurements between various photogrammetric platforms to evaluate their suitability for snow depth retrieval considering various factors such as continuity, mapping scale, etc., and observed that accuracy of the retrieved snow depth increases with an increase in spatial resolution of the sensor.

5.2. Methods based on active microwave remote sensing

5.2.1. Estimation of snow permittivity, LWC, and snow density

The fundamental procedure for the retrieval of SGP using microwave remote sensing is based on the modeling of surface and volume scattering of the snowpack. Shi and Dozier (1995) proposed an algorithm for the inversion of snow wetness using C-band polarimetric SIR-C/X-SAR datasets by considering both the surface and the volume scattering. This algorithm utilizes a simplified surface backscattering model based on the numerical simulations for wet snow conditions. The volume scattering ratio in copolarization channels was determined to retrieve the snow permittivity (Shi and Dozier 1995). Studies based on this approach modeled the estimates of the snow density, snow depth, equivalent grain size, and dielectric constant of the snow cover, along with the roughness of the underlying soil or rock using backscattering information in the VV and HH polarization at L-band frequency (1.25 GHz) (Shi and Dozier 2000a, 2000b). Further, a modified-Shi inversion was introduced for estimating snow density and snow wetness (Negi et al. 2013).

Fung and Chen (2010) introduced the Integral Equation Model (IEM) as an advancement of the small perturbation model for characterizing the bare earth surfaces. The IEM characterizes bare smooth

surfaces using various parameters including: the incidence angle, polarization, and radar wavelength (λ), and the target parameters like dielectric constant (ϵ_r), the standard deviation of surface height (H_{rms}), the correlation function, and the correlation length (L) (Fung and Chen 2010). Various studies applied IEM based approaches for snow parameters retrieval (Bhattacharya et al. 2014; Awasthi et al. 2020). The IEM was primarily used in these methods to model the Fresnel coefficients that are related to the real part of the permittivity. The Fresnel transmission coefficients in the horizontal direction (γ_{HH}) and in the vertical direction (γ_{VV}) are the function of incidence angle, and the dielectric constant of the medium (ϵ_s) expressed in equation (5) (Der et al. 2001; Fung and Chen 2010).

$$\begin{aligned}\gamma_{HH} &= \frac{2 \cos \theta_i}{\cos \theta_i + \sqrt{\epsilon_s - \sin^2 \theta_i}}, \\ \gamma_{VV} &= \frac{2 \sqrt{\epsilon_s - \sin^2 \theta_i}}{\epsilon_s \cos \theta_i + \sqrt{\epsilon_s - \sin^2 \theta_i}}\end{aligned}\quad (5)$$

Baghdadi et al. (2016) developed a framework of a semi-empirical radar backscattering model for modeling the backscatter from the bare surfaces. In a study by Varade et al. (2019), the LWC determined by Baghdadi et al. (2016) and Surendar et al. (2015) was compared using RADARSAT-2 data. It included three primary parameters: incidence angle, surface moisture, and the surface roughness given by RMS height.

$$\begin{aligned}a_{HH} &= \frac{\cos \theta_i - \sqrt{\epsilon_s - \sin^2 \theta_i}}{\cos \theta_i + \sqrt{\epsilon_s - \sin^2 \theta_i}}, \\ a_{VV} &= \frac{(\epsilon_s - 1)\sin^2 \theta_i - \epsilon_s(1 + \sin^2 \theta_i)}{\left(\epsilon_s \cos \theta_i + \sqrt{\epsilon_s - \sin^2 \theta_i}\right)^2}\end{aligned}\quad (6)$$

In Surendar et al. (2015), the snow LWC was modeled using the Fresnel transmission coefficients and the Bragg's reflection coefficients accounting for the volume and the surface scattering. In this approach, the Fresnel transmission coefficients and the Bragg's reflection coefficients shown in equation (5) and (6) were modeled using the G4U decomposition of the coherency matrix. In equations (5) and (6), ϵ_s represents the volume and the surface permittivity of snow, respectively. The RMSE between the modeled results of Baghdadi et al. (2016) and Surendar et al. (2015) was observed to be more than 1% by

volume, indicating the inefficiency of the model by Baghdadi et al. (2016) for dry snow. According to Baghdadi et al. (2016), the relationship between the radar backscattering coefficient σ_0 and the surface parameters (roughness and moisture) for the bare surface is represented in equation (7) as follows:

$$\sigma_{pq}^0 = \delta(\cos\theta)^\beta 10^{\gamma \cotan(\theta)mv} (kH_{rms})^{\xi \sin\theta} \quad (7)$$

where θ is the incident angle, H_{rms} is the RMS height. δ , β , γ , and ξ are the coefficients estimated for each radar polarization, applying the technique of least squares by minimizing the sum of squares of the differences between the measured and modeled radar signal. The approach by Baghdadi et al. (2016) is an extension of the Dubois model, which provides estimates of only the co-polarization backscatter. Snehmani, Nigam, and Singh (2010) developed an inversion model for estimating the dry snow density using ENVISAT-ASAR dual co-polarization datasets. Surendar et al. (2015) determined the snowpack volume density using an empirical model based on the permittivity. The permittivity was derived from the inversion of the Fresnel transmission coefficients based on the G4U transformed coherency matrix.

Singh et al. (2017) proposed the utilization of the Generalized Singh-Cloude 3-component hybrid decomposition method (GS3H) for the estimation of snow density. The GS3H decomposition scheme incorporates an extended volume scattering model that is generalized by considering uniformly distributed spheroidal snow particles as volume scatterers. The experiments for the retrieval of snow density using the GS3H-based approach were carried out using the fully polarimetric TerraSAR-X data, and their results were observed to promising for dry snow.

Varade et al. (2020c) demonstrated that the surface scattering component for old snow is not negligible. Therefore, the effective density of the snowpack should be estimated by considering both the surface and the volume scattering components. In this study, experiments were conducted using two different approaches. In the first approach that utilizes the decomposition-based methods, the G4U and the GS3H-based strategies were used for computing the effective permittivity. The effective permittivity of the snowpack is determined as the weighted sum of the surface and the volume permittivity, which are estimated using the Fresnel transmission and reflection

coefficients. In the second approach, Varade et al. (2020c)modeled the snow permittivity estimates by utilizing the incremental/decremental scattering factors based on the total modified Mueller matrix and the attenuation constants. The scattering factors are determined using the bi-temporal 3×3 covariance matrices. The attenuation constants were determined using the radar range equation, assuming exponential decay of the radar signal in the snowpack. The snow density, in this case, was determined using the Matzler's empirical model (Mätzler 1996). In this study, it was observed that the proposed approach showed significantly better performance than the decomposition-based methods for old snow. Further, the proposed approach was also observed to be relatively robust to changes in the liquid water content and the snow depth.

In the methods discussed above, the permittivity of the snowpack plays a significant role as it is one of the important parameters for modeling the snow density or the LWC (Looyenga 1965; Denoth 1994; Mätzler 1996). Manickam et al. (2016) proposed a novel methodology for the estimation of snow surface dielectric constant by introducing the optimum degree of polarization. In this study, the ratio of Bragg's scattering coefficients B_{HH} and B_{VV} as a function of the local incidence angle (θ_i) and the snowpack dielectric constant (ϵ_r) are related to the dominant scattering angle (a_s). A summary of the various methods in the literature for the estimation of SGP including the dielectric constant, wetness, and density is shown in Table 3, and the various methods in for the estimation of snow depth and SWE are shown in Table 4.

5.2.2. Estimation of snow depth/SWE

For the regional scale estimation of snow depth, active microwave remote sensing-based techniques have a definite edge over the coarse resolution passive microwave remote sensing techniques. The algorithm for estimating snow water equivalence was developed using VV and HH polarization information of SIR-C/X-SAR datasets (Shi and Dozier 2000a, 2000b). Further, Shi (2006) developed a numerical simulations-based approach for evaluating its feasibility to estimate X band and Ku-band datasets. Leinss, Parrella, and Hajnsek (2014) demonstrated a significant correlation between the co-polarized phase difference between VV and HH channels with

respect to the depth of fresh snow using polarimetric X-band SAR datasets.

Various studies have utilized SAR Interferometry based techniques for analyzing surface dynamics, particularly surface subsidence. Guneriussen et al. (2001) demonstrated changes in snow water equivalent (SWE) with respect to the differential interferometric phase. The phase shift and the snow mass accumulated during the period of snow-free and snow covered images are related based on the geometrical and physical properties of the snowpack (Guneriusen et al. 2001; Rott, Nagler, and Scheiber 2004). (Liu et al. 2017) incorporated the auxiliary information from the in-situ sites or from the snow observation stations in the InSAR-based estimation of snow depth, which demonstrated a significant improvement in the estimated results. Li et al. (2017) proposed an approach for efficient estimation of snow depth parameter from the differential interferometric (DInSAR) phase by calibrating the snow density parameter and replacing incidence angle by local incidence angle. Lievens et al. (2019) demonstrated a modeling approach for estimating snow depth across the northern-hemisphere mountains using time-series Sentinel-1 datasets.

Varade et al. (2020b) proposed a bias correction method for improving differential interferometric SAR (DInSAR) based snow depth estimates. In this study, two bias corrections are introduced; for the snow phase, and the residual errors. The snow depth is computed as the scale-adjusted weighted sum of the improved DInSAR displacements in the VV and the VH channels. Mahmoodzada, Varade, and Shimada (2020) proposed an extension of the study by Varade et al. (2020c) for the Khanabad watershed in Afghanistan. In this study, the effect of the dry snow volume scattering is incorporated in the DInSAR displacement rather than the snow phase. In this case, to account for the effect of the dry snow volume scattering, the spatially distributed snowpack permittivity determined based on Varade et al. (2020c) using Sentinel-1 data is utilized. Patil et al. (2020) utilized the PollnSAR Coherence information based on bistatic TerraSAR-X datasets for the estimation of the Snow Depth and Snow water equivalent. In another approach, the co-polar phase difference and the particle anisotropy was used to model the snow depth (Patil, Singh, and Rüdiger 2020). Awasthi et al. (2021) proposed PollnSAR inversion modeling-based

approach for snow depth estimation using pursuit mono-static TerraSAR-X/TanDEM datasets.

5.3. Methods based on passive microwave remote sensing

Typically, studies utilizing passive microwave data make use of dual-frequency brightness temperatures to empirically estimate SWE (Chang, Foster, and Hall 1987; Derksen 2008). In several studies, the spectral difference approach has been used to determine the SWE empirically, based on the 18 GHz and 37 GHz channels (Kunzi, Patil, and Rott 1982). Chang, Foster, and Hall (1987) introduced a scaling factor in the spectral difference approach, which accounted for the standard snow grain size of 0.3 mm and a density of 0.3 Kg/dm³. Hallikainen (1989) introduced the spectral polarization difference by incorporating vertical polarization channels along with the conventional horizontal polarization channels in the spectral differencing approach. Derksen (2008) defined the relationship between the vertically polarized passive microwave brightness temperature and the SWE. A noteworthy inference from this study was the higher correlation of the 18.7–10.7 GHz brightness temperature difference compared to the 36.5–18.7 GHz brightness temperature difference in the forested regions of Manitoba, Canada. Foster et al. (2005) developed an approach by incorporating an error estimation method based on the snow morphology for the estimation of SWE. Che et al. (2016) incorporated an estimate of the forest transmissivity for improving the snow depth estimates.

In several studies, the conventional linear regression used to model the SWE based on the spectral differencing approach empirically has been replaced by machine learning-based regression. Tsang et al. (1992) simulated the mean snow grain size, snow density, and snow temperature by utilizing an artificial neural network trained by a dense-media multiple-scattering model. Tedesco et al. (2004) utilized the artificial neural network for the estimation of snow depth and SWE from SSM/I passive microwave data. Dariane, Azimi, and Zakerinejad (2014) determined the SWE using an integrated model comprising the wavelet transform and the ANN. Liang et al. (2015) utilized the support vector machines for the estimation of snow depth by integrating the microwave brightness temperature with visible infrared

reflectance. Xiao et al. (2018) developed a support vector machine regression-based approach for the retrieval of snow depth that accounted for three snow cover stages and four land cover types.

6. Current challenges, limitations, and future prospects in remote sensing of snow

Remote sensing techniques have been significantly utilized in the monitoring of alpine snow at various levels throughout the electromagnetic spectrum. However, depending upon the sensors and their corresponding operability in the specific spectrum, several benefits and hindrances exist (Dietz et al. 2012; Tsai et al. 2019). Due to the extensive cloud cover in the winter season in the mountainous regions, the applicability of the optical remote sensing data is highly constrained and is dependent predominantly upon the availability of cloud-free scenes (Marshall, Dowdeswell, and Rees 1994). Furthermore, the applicability of the optical remote sensing data including multispectral and hyperspectral is limited to qualitative analysis of the snow cover (Snehmani et al. 2015; Varade, Sure, and Dikshit 2019). Although methods to characterize snow surface quantitatively exist in the literature (Eppanapelli et al. 2018; Varade and Dikshit 2019), these methods do not differentiate between the wet snow from the refrost snow that is a common issue in the alpine snowpack in the visible and infrared spectrum.

Dozier et al. (2009) indicated the suitability of the NIR wavelengths in the spectral range of 980–1030 nm for differentiating the wet snow from the refrost snow. However, this spectrum is typically only covered in hyperspectral data. In essence, the potential of the methodology proposed by Eppanapelli et al. (2018) and Varade and Dikshit (2019) for quantitatively characterizing the snow geophysical parameters could be significantly improved by replacing the existing NIR bands by one that lies within this spectral range. It is evident that present multispectral sensors lack any bands within this spectral range, and this constitutes a valid factor for designing future optical land remote sensing missions. Similar to multispectral/hyperspectral sensors, thermal sensors are also limited in their applicability corresponding to the availability of the cloud-free scenes. Moreover, the surface temperature sensitivity exhibited by these sensors are not sufficient for the

characterization of the snow surface processes (Dozier and Warren 1982). Furthermore, the space-borne thermal sensor data available to date and planned in future such as the Trishna mission based on the joint cooperation of CNES and ISRO (<https://www.theia-land.fr/en/trishna-a-franco-indian-mission-to-monitor-the-water-status-of-continental-ecosystems/>) is/will be available at spatial resolution in the range of 57–90 m., which could be suitable for monitoring the spatio-temporal dynamics of the snow surface on a regional scale. It is expected that such studies will be carried out in the recent future. However, in general, it is easily noticeable that optical remote sensing does not exhibit the all-weather capability of the microwave sensors and falls well short from the capabilities demonstrated by the microwave sensors for snow studies.

Although passive microwave sensor systems exhibit the all-weather capability and to add higher repeatability due to their operational constraints, they are only able to generate products that are possible at significantly coarser resolutions (Koike and Suhama 1993). Evidently, these sensors do not provide moderate-resolution products where the spatial resolution is of the order or hundreds of meters. Due to this, inter-calibration of passive microwave snow products with moderate resolution products becomes a highly complicated process introducing significant biases due to the differences in the spatial resolution. Thus, for a regional-scale analysis of the snowpack, spatial downscaling schemes based on artificial intelligence or machine learning have become popular in the recent years (Zhu et al. 2021) owing to the fact that these products are available at a relatively better temporal resolution. However, the application of such methods is a complex process and is possible typically at relatively large scales. Further, this is dependent upon the availability and the volume of the field measurements available from campaigns or from ground stations. Due to the rugged terrain in the alpine regions, spatially distributed campaigns and are difficult to be organized, and concurrent campaigns at the same site do not provide suitable data. Additionally, the separability between consecutive ground stations is usually not uniform, leading to upscaling errors.

One of the major problems with the earlier space-borne active microwave systems was the lower temporal revisit. Table A1 summarizes the specifications

of some of the widely used spaceborne SAR satellite missions that have been extensively used in the studies of snow. With recent missions like the Sentinel-1 (http://www.esa.int/Applications/Observing_the_Earth/Copernicus/Sentinel-1), this has been accounted for, where the revisit period is typically 6–7 days (including both 1A and 1B). However, since the Sentinel-1, data acquisition scheme incorporates a recording of bursts in each swath (three swaths in Interferometric Wide mode combined into one product), the computational complexity for a regional scale analysis is relatively higher. Yet, the C-band Sentinel-1 dual polarimetric and interferometric SAR data have found significant applications in snow/ice studies owing to free availability to the research community. With missions like NASA-ISRO SAR (NISAR, <https://nisar.jpl.nasa.gov/>) coming up providing data at L-band and S-band, there is significant scope for utilization of multi-frequency multi-sensor data for snow studies, particularly considering the higher penetrability of the L-band SAR in the snowpack. Additionally, NISAR data is also expected to be delivered under full polarimetric (Quad Pol) configurations for the L-band yielding significant opportunities for the research community. Table A2 summarizes the specifications of some of the spaceborne active microwave satellites that exhibit significant potential for the studies of snow.

The interferometric and the polarimetric capabilities of these sensors enable us to predict relatively precisely the snowpack parameters such as the depth and the SWE (Varade et al. 2020b; Mahmoodzada, Varade, and Shimada 2020). However, only for the early winter season where the snowpack is dry. During the melt season, the determination of the SWE and the snow depth is still difficult due to the presence of liquid water content, which significantly affects the effective permittivity of the snowpack (Mahmoodzada, Varade, and Shimada 2020). Subsequently, the snow refraction model discussed in section 3.2.2 does not hold. While the estimates of SWE are significant for runoff and discharge studies in the alpine catchments, their determination in the melt season still requires significant efforts in developing new approaches. With the possibility of multi-frequency data, it could be possible to direct efforts from the research community in this regard. Additionally, fully polarimetric and interferometric SAR data could be highly useful considering that the

recent literature revealed the application of fully polarimetric SAR data for efficient estimation of snow density (Varade et al. 2020a). Such capabilities are now possible with the NISAR mission. However, as compared to the popular polarimetric SAR sensors, research in the aligned directions is yet limited based on compact polarimetric sensors such as the RISAT-I, but could be expected when more data is available, for example, from the RADARSAT Constellation Mission (<https://www.asc-csa.gc.ca/eng/satellites/radarsat/default.asp>). It is worth mentioning that the data from these missions are expected to be available commercially. Besides these, similar upcoming missions are in progress, including Tandem-L, like the L-band version of the TerraSAR/Tandem-X mission, ALOS PALSAR-3 etc.

The regional climate affects the patterns of snowfall (relating to snow accumulation and depth), dynamics of SCA, and the timing of the snowmelt, particularly influencing the downstream areas in the alpine regions (Pomeroy 2007). Additionally, the accumulation of windblown snow (typically, from the windward to the lee-way side) introduces uncertainties in the SGP estimates derived using remote sensing. Due to the heterogeneous nature of such accumulation, the medium resolution to coarser resolution satellite products is incapable of producing precise estimates of snow depth and density. The wind-influenced snowdrifts also introduce spatio-temporal variations in the SCA and in some cases, also introduce thermal gradients in the snowpack (Fierz and Baunach 2000; Shao et al. 2017). As mentioned earlier, the variations in the regional climate, mainly temperature, affect the snow metamorphism, thus altering the SGP such as the density and SWE. Often this results in the development of ice crusts and depth hoar in the snowpack (Colbeck 1982). Since most of the methods based on microwave remote sensing consider a two-layer snowpack model, these differences in the attributes of individual layers are not replicated in the derived estimates, and only the approximate effective information is retrievable for the snowpack (Varade et al. 2020a).

The regional topography also affects the information retrieved using remote sensing by introducing uncertainties. The effect of slope and aspect is critical in the precise determination of SCA using optical remote sensing due to the differences of solar radiation received by the different aspects (Zhao et al.

2015). This follows further for InSAR-based methods, where the steeplines exhibit significant uncertainty in the estimates of snow depth (Varade et al. 2020b). The PM brightness temperature used in the empirical retrieval of SWE is also affected significantly by the interactive radiation between different terrain features, shadows, and the changes in elevation (Mätzler 2006). The presence of forests and vegetation also affect significantly both the PM and active microwave signal retrievals. In PM remote sensing, the presence of boreal forests results in significant underestimation of SWE due to the mixing of radiation from snow (Chang et al. 1996). Topography with significant relief (>500 m) also affects the brightness temperature (in case of PM) (Foster et al. 2005) and the backscatter (in case of active RS) (Varade et al. 2020c). The orientation of the mountains corresponding to the satellite geometry also significantly affects the backscatter (Varade et al. 2020c).

7. Conclusion

On a regional scale, snowpack monitoring is significant considering the various aspects involved in environmental studies, regional climate studies, water resource management, and disaster risk reduction and management pertaining to the case of an avalanche. At global scales, the monitoring of snow is essential for climate modeling and studying the evolution of Earth's energy budget. Snow is a highly incoherent medium. Subsequently, for the monitoring of snowpack, precise and timely information on the SGP is vital with regard to the aforementioned areas.

Remote sensing has played a significant role in facilitating snowpack monitoring. With the increase in the availability of remote sensing data, a corresponding surge has been observed in the development of methods for the quantitative and qualitative studies of the SGP. However, each of these methods is constrained by the limitations of the sensor used in the acquisition of the remote sensing data. Although we have observed methods providing relatively good estimates of SGP, the primary issue with optical remote sensing is related to the penetrability of the signal in the snowpack, thus rendering information pertaining to the snow surface only. Overall, qualitatively, optical remote sensing can provide precise information on the snow cover.

In contrast to optical remote sensing, the microwave signal penetrates deep into the snowpack providing key information regarding the volumetric snowpack characteristics. However, the penetration of the signal is largely dependent upon the incidence of the signal, the LWC in the snowpack, and the frequency of the microwave signal. Although several methods have been able to retrieve precise information on the SGP quantitatively, these methods are constrained by several assumptions, including the snowpack to be dry or wet. In contrast, in the mid-winter season in the alpine regions, it could be said that the snowpack is between dry and wet, as there is some LWC ~1%–2% vol. in the old/settled snow, which occurs due to periodical melt and refrost processes. For such a snowpack, thus, there is a significant need to develop methods that accurately determine the SGPs. Additionally, there is also a considerable need to develop robust mathematical inter-relations between the SGP for the case of old snow.

Disclosure statement

The authors declare that they have no known competing financial interests or personal relationships that could have appeared to influence the work reported in this paper.

ORCID

Shubham Awasthi  <http://orcid.org/0000-0002-1624-3301>
Divyesh Varade  <http://orcid.org/0000-0003-0283-8387>

Data Availability Statement

The data for the spectral response curves illustrated in this manuscript are freely available from the ASTER spectral library at <https://speclib.jpl.nasa.gov/>.

References

- Adams, M. S., Y. Bühler, and R. Fromm. 2018. "Multitemporal Accuracy and Precision Assessment of Unmanned Aerial System Photogrammetry for Slope-Scale Snow Depth Maps in Alpine Terrain." *Pure Appl Geophys* 175 (9): 3303–3324. doi:10.1007/s00024-017-1748-y.
- Aguirre, F., J. Carrasco, T. Sauter, C. Schneider, K. Gaete, E. Garín, R. Adaros, N. Butorovic, R. Jaña, and G. Casassa 2018. Snow Cover Change as a Climate Indicator in Brunswick Peninsula,

- Patagonia. *Front Earth Science* <https://www.frontiersin.org/article/10.3389/feart.2018.00130/full>
- Akhtar, M., N. Ahmad, and M. J. Booij. 2008. "The Impact of Climate Change on the Water Resources of Hindu Kush-Karakorum-Himalaya Region under Different Glacier Coverage Scenarios." *J Hydrology* 355 (1–4): 148–163. doi:[10.1016/j.jhydrol.2008.03.015](https://doi.org/10.1016/j.jhydrol.2008.03.015).
- Anisimov, O. A., D. G. Vaughan, T. V. Callaghan, C. Furgal, H. Marchant, T. D. Prowse, H. Vilhjálmsson, and J. E. Walsh. 2007. "Polar Regions (Arctic and Antarctic)." *Climate Change* 15: 653–685.
- Awasthi, S., P. K. Thakur, S. Kumar, A. Kumar, K. Jain, and S. Mani. 2020. "Snow Density Retrieval Using Hybrid Polarimetric RISAT-1 Datasets." *IEEE Journal of Selected Topics in Applied Earth Observations and Remote Sensing* 13: 3058–3065.
- Awasthi, S., S. Kumar, P. K. Thakur, K. Jain, A. Kumar, and Snehmani. 2021. "Snow Depth Retrieval in North-Western Himalayan Region Using Pursuit-monostatic TanDEM-X Datasets Applying Polarimetric Synthetic Aperture Radar Interferometry Based Inversion Modelling." *Int J Remote Sensing* 42 (8): 2872–2897. <https://www.tandfonline.com/doi/full/10.1080/01431161.2020.1862439>.
- Baba, M. W., S. Gascoin, O. Hagolle, E. Bourgeois, C. Desjardins, and G. Dedieu. 2020. "Evaluation of Methods for Mapping the Snow Cover Area at High Spatio-temporal Resolution with VENµS." *Remote Sensing* 12 (18): 3058. www.mdpi.com/journal/remotesensing.
- Baggi, S., and J. Schweizer. 2009. "Characteristics of Wet-snow Avalanche Activity: 20 Years of Observations from a High Alpine Valley (Dischma, Switzerland)." *Natural Hazards* 50 (1): 97–108.
- Baghdadi, N., M. Choker, M. Zribi, M. Hajj, S. Paloscia, N. Verhoest, H. Lievens, F. Baup, and F. Mattia. 2016. "A New Empirical Model for Radar Scattering from Bare Soil Surfaces." *Remote Sensing* 8 (11): 920. <http://www.mdpi.com/2072-4292/8/11/920>.
- Baghdadi, N., and M. Zribi. 2006. "Evaluation of Radar Backscatter Models IEM, OH and Dubois Using Experimental Observations." *Int J Remote Sensing* 27 (18): 3831–3852. <https://www.tandfonline.com/doi/full/10.1080/01431160600658123>.
- Baldridge, A. M., S. J. Hook, C. I. Grove, and G. Rivera. 2009. "The ASTER Spectral Library Version 2.0." *Remote Sensing of Environment* 113 (4): 711–715.
- Barros, A. P., and D. P. Lettenmaier. 1994. "Dynamic Modeling of Orographically Induced Precipitation." *Rev Geophys* 32 (3): 265. doi:[10.1029/94RG00625](https://doi.org/10.1029/94RG00625).
- Bellaire, S., A. van Herwijnen, C. Mitterer, and J. Schweizer. 2017. "On Forecasting Wet-snow Avalanche Activity Using Simulated Snow Cover Data." *Cold Regions Science and Technology* 144: 28–38.
- Bellaire, S., J. B. Jamieson, and C. Fierz. 2011. "Forcing the Snow-cover Model SNOWPACK with Forecasted Weather Data." *Cryosphere* 5 (4): 1115–1125.
- Bender, E., M. Lehning, and J. Fiddes. 2020. "Changes in Climatology, Snow Cover, and Ground Temperatures at High Alpine Locations." *Front Earth Sci* 8: 100. <https://www.frontiersin.org/article/10.3389/feart.2020.00100/full>.
- Berman, E. E., D. K. Bolton, N. C. Coops, Z. K. Mityok, G. B. Stenhouse, and R. D. Moore. 2018. "Daily Estimates of Landsat Fractional Snow Cover Driven by MODIS and Dynamic Time-warping." *Remote Sensing of Environment* 216: 635–646.
- Bernier, M., J. P. Dedieu, Y. Duguay, and G. Seguin. 2017. "Snow Water Equivalent Estimation Using High Resolution SAR Data." In: *IEEE International Geoscience and Remote Sensing Symposium* Vol. 2017-July 23–28, Fort Worth, Texas, USA.
- Bernier, P. Y. 1987. "Microwave Remote Sensing of Snowpack Properties: Potential and Limitations." *Nord Hydrology* 18 (1): 1–20. <https://iwaponline.com/hr/article-pdf/18/1/1/2372/1.pdf>.
- Bhattacharya, A., M. Surendar, S. De, G. Venkataraman, and G. Singh. 2014. "Snow Wetness Estimation from Dual Polarimetric Coherent TerraSAR-X Data." In: 2014 IEEE International Geosci Remote Sens Sympium July 13–18, 2017, Quebec City, Canada, p. 2766–2769. <http://ieeexplore.ieee.org/document/6947049/>
- Bian, J., A. Li, Q. Liu, and C. Huang. 2016. "Cloud and Snow Discrimination for CCD Images of HJ-1A/B Constellation Based on Spectral Signature and Spatio-Temporal Context." *Remote Sensing* 8 (1): 31.
- Bokhorst, S., S. H. Pedersen, L. Brucker, O. Anisimov, J. W. Bjerke, R. D. Brown, D. Ehrlich, et al. 2016. "Changing Arctic Snow Cover: A Review of Recent Developments and Assessment of Future Needs for Observations, Modelling, and Impacts." *Ambio* 45 (5): 516–537. www.kva.se/en.
- Bookhagen, B., and D. W. Burbank. 2010. "Toward a Complete Himalayan Hydrological Budget: Spatiotemporal Distribution of Snowmelt and Rainfall and Their Impact on River Discharge." *J Geophys Res Earth Surf* 115: 3.
- Brown, R. D., and D. A. Robinson. 2005. "Snow and Snow Cover." In *Encycl World Climatol*, edited by J. E. Oliver, 658–663. Dordrecht: Springer Netherlands. doi:[10.1007/1-4020-3266-8_187](https://doi.org/10.1007/1-4020-3266-8_187).
- Bühler, Y., M. Marty, L. Egli, J. Veitinger, T. Jonas, P. Thee, and C. Ginzler. 2015. "Snow Depth Mapping in High-alpine Catchments Using Digital Photogrammetry." *Cryosphere* 9 (1): 229–243.
- Callaghan, T. V., M. Johansson, R. D. Brown, P. Y. Groisman, N. Labba, V. Radionov, R. S. Bradley, et al. 2011. "Multiple Effects of Changes in Arctic Snow Cover." *Ambio* 40 (SUPPL.1): 32–45.
- Chang, A. T. C., J. L. Foster, and D. K. Hall. 1987. "Nimbus-7 SMMR Derived Global Snow Cover Parameters." *Annals of Glaciology* 9: 39–44.
- Chang, P. S., J. B. Mead, E. J. Knapp, G. A. Sadowy, R. E. Davis, and R. E. McIntosh. 1996. "Polarimetric Backscatter from Fresh and Metamorphic Snowcover at Millimeter Wavelengths." *IEEE Transactions on Antennas and Propagation* 44 (1): 58–73.
- Chang, T. C., P. Gloersen, T. Schmugge, T. T. Wilheit, and H. J. Zwally. 1976. "Microwave Emission from Snow and Glacier Ice." *Journal of Glaciology* 16 (74): 23–39.

- Che, T., L. Dai, X. Zheng, X. Li, and K. Zhao. 2016. "Estimation of Snow Depth from Passive Microwave Brightness Temperature Data in Forest Regions of Northeast China." *Remote Sensing of Environment* 183: 334–349.
- Cloude, S. R. 2010. *Polarisation Applications in Remote Sensing*. New York: Oxford University Press.
- Colbeck, S. C. 1982. "An Overview of Seasonal Snow Metamorphism." *Rev Geophys* 20 (1): 45.
- Da Ronco, P., and C. De Michele. 2014. "Cloud Obstruction and Snow Cover in Alpine Areas from MODIS Products." *Hydrol Earth Syst Sci* 18 (11): 4579–4600. <https://hess.copernicus.org/articles/18/4579/2014/>.
- Dariane, A. B., S. Azimi, and A. Zakerinejad. 2014. "Artificial Neural Network Coupled with Wavelet Transform for Estimating Snow Water Equivalent Using Passive Microwave Data." *J Earth Syst Sci* 123 (7): 1591–1601.
- De, S., A. Muhuri, S. Manickam, and A. Bhattacharya. 2018. "Snow Cover Mapping with Poincaré Sphere Parameters from Polaris Images Using an Auto-encoder Network." In *IGARSS 2018-2018 IEEE International Geoscience and Remote Sensing Symposium*, pp. 8086–8089. 2018-July.
- DeBeer, C. M., and J. W. Pomeroy. 2017. "Influence of Snowpack and Melt Energy Heterogeneity on Snow Cover Depletion and Snowmelt Runoff Simulation in a Cold Mountain Environment." *J Hydrol* 553: 199–213.
- Denoth, A. 1994. "An Electronic Device for Long-term Snow Wetness Recording." *Annals of Glaciology* 19: 104–106.
- Der, W. T., K. S. Chen, J. Shi, and A. K. Fung. 2001. "A Transition Model for the Reflection Coefficient in Surface Scattering." *IEEE Transactions on Geoscience and Remote Sensing : A Publication of the IEEE Geoscience and Remote Sensing Society* 39 (9): 2040–2050.
- Derkzen, C. 2008. "The Contribution of AMSR-E 18.7 And 10.7 GHz Measurements to Improved Boreal Forest Snow Water Equivalent Retrievals." *Remote Sensing of Environment* 112 (5): 2701–2710.
- Derkzen, C., A. Walker, and B. Goodison. 2003. "A Comparison of 18 Winter Seasons of in Situ and Passive Microwave-derived Snow Water Equivalent Estimates in Western Canada." *Remote Sensing of Environment* 88 (3): 271–282.
- Deschamps-Berger, C., S. Gascoin, E. Berthier, J. Deems, E. Gutmann, A. Dehecq, D. Shean, and M. Dumont. 2020. "Snow Depth Mapping from Stereo Satellite Imagery in Mountainous Terrain: Evaluation Using Airborne Laser-scanning Data." *Cryosphere* 14 (9): 2925–2940.
- Dietz, A. J., C. Kuenzer, U. Gessner, and S. Dech. 2012. "Remote Sensing of Snow - a Review of Available Methods." *International Journal of Remote Sensing* 33 (13): 4094–4134.
- Dozier, J. 1989. "Spectral Signature of Alpine Snow Cover from the Landsat Thematic Mapper." *Remote Sensing of Environment* 28: 9–22.
- Dozier, J., R. O. Green, A. W. Nolin, and T. H. Painter. 2009. "Interpretation of Snow Properties from Imaging Spectrometry." *Remote Sensing of Environment* 113: S25–S37.
- Dozier, J., and S. G. Warren. 1982. "Effect of Viewing Angle on the Infrared Brightness Temperature of Snow." *Water Resources Research* 18 (5): 1424–1434.
- Dozier, J., and T. H. Painter. 2004. "Multispectral and Hyperspectral Remote Sensing of Alpine Snow Properties." *Annual Review of Earth and Planetary Sciences* 32 (1): 465–494.
- Eberhard, L. A., P. Sirguey, A. Miller, M. Marty, K. Schindler, A. Stoffel, and Y. Bühler. 2020. "Intercomparison of Photogrammetric Platforms for Spatially Continuous Snow Depth Mapping." *The Cryosphere* 15 (1): 69–94.
- Ellerbruch, D. A., and H. S. Boyne. 1980. "Snow Stratigraphy and Water Equivalence Measured with an Active Microwave System." *Journal of Glaciology* 26 (94): 225–233.
- Eppanapelli, L. K., N. Lintzén, J. Casselgren, and J. Wählén. 2018. "Estimation of Liquid Water Content of Snow Surface by Spectral Reflectance." *J Cold Reg Eng* 32 (1): 5018001–5018007.
- Ferro-Famil, L., E. Pottier, J. Saillard, J. P. Dedieu, M. Bernier, and J. P. Fortin. 1999. "The Potential of Full Polarimetric SAR Data to Classify Dry Snowcover." In *Int Geosci Remote Sens Symp. IGARSS'99*, Vol. 3, IEEE. 1792–1794.
- Fierz, C., and T. Baunach. 2000. "Quantifying Grain-shape Changes in Snow Subjected to Large Temperature Gradients." *Annals of Glaciology* 31: 439–444.
- Fischer, J. T. 2013. "A Novel Approach to Evaluate and Compare Computational Snow Avalanche Simulation." *Natural Hazards and Earth System Sciences* 13 (6): 1655–1667.
- Foster, J. L., C. Sun, J. P. Walker, R. Kelly, A. Chang, J. Dong, and H. Powell. 2005. "Quantifying the Uncertainty in Passive Microwave Snow Water Equivalent Observations." *Remote Sensing of Environment* 94 (2): 187–203.
- Fung, A. K., and K. S. Chen. 2010. *Microwave Scattering and Emission Models for Users*. Norwood, MA: Artech House.
- Gascoin, S., M. Grizonnet, M. Bouchet, G. Salgues, and O. Hagolle. 2019. "Theia Snow Collection: High-resolution Operational Snow Cover Maps from Sentinel-2 and Landsat-8 Data." *Earth Syst Sci Data* 11 (2): 493–514.
- Gascoin, S., Z. Barrou Dumont, C. Deschamps-Berger, F. Marti, G. Salgues, J. I. López-Moreno, J. Revuelto, T. Michon, P. Schattan, and O. Hagolle. 2020. "Estimating Fractional Snow Cover in Open Terrain from Sentinel-2 Using the Normalized Difference Snow Index." *Remote Sensing* 12 (18): 2904. <https://www.mdpi.com/2072-4292/12/18/2904>.
- Goetz, J., and A. Brenning. 2019. "Quantifying Uncertainties in Snow Depth Mapping from Structure from Motion Photogrammetry in an Alpine Area." *Water Resources Research* 55 (9): 7772–7783.
- Grody, N. 2008. "Relationship between Snow Parameters and Microwave Satellite Measurements: Theory Compared with Advanced Microwave Sounding Unit Observations from 23 to 150 GHz." *Journal of Geophysical Research* 113 (D22): D22108. doi:10.1029/2007JD009685.
- Guneriusson, T., H. Ka, H. Johnsen, and I. Lauknes. 2001. "InSAR for Estimation of Changes in Snow Water Equivalent of Dry Snow." *IEEE Transactions on Geoscience and Remote Sensing : A Publication of the IEEE Geoscience and Remote Sensing Society* 39 (10): 2101–2108.
- Gupta, R. P., U. K. Haritashya, and P. Singh. 2005. "Mapping Dry/wet Snow Cover in the Indian Himalayas Using IRS

- Multispectral Imagery." *Remote Sensing of Environment* 97 (4): 458–469.
- Hall, D. K., A. Frei, and S. J. Déry. 2014. "Remote Sensing of Snow Extent." In *Remote Sensing of the Cryosphere*, edited by M. Tedesco, 31–47. Chichester, UK: Wiley Blackwell.
- Hall, D. K., G. A. Riggs, and V. V. Salomonson. 1995. "Development of Methods for Mapping Global Snow Cover Using Moderate Resolution Imaging Spectroradiometer Data." *Remote Sensing of Environment* 54 (2): 127–140.
- Hall, D. K., J. L. Foster, D. L. Verbyla, A. G. Klein, and C. S. Benson. 1998. "Assessment of Snow-cover Mapping Accuracy in a Variety of Vegetation-cover Densities in Central Alaska." *Remote Sensing of Environment* 66 (2): 129–137.
- Hallikainen, M. 1992. "Review of the Microwave Dielectric and Extinction Properties of Sea Ice and Snow." In *Int Geosci Remote Sens Symp.*, Houston, TX, Vol. 2, Institute of Electrical and Electronics Engineers . 961–965.
- Hallikainen, M. T. 1989. "Microwave Radiometry of Snow." *Adv Sp Res* 9 (1): 267–275.
- Hallikainen, M. T., F. T. Ulaby, and T. E. Van Deventer. 1987. "Extinction Behavior of Dry Snow in the 18-to 90-GHz Range." *IEEE Transactions on Geoscience and Remote Sensing*(6): 737–745.
- Haq, M. A., A. Ghosh, G. Rahaman, and P. Baral. 2019. "Artificial Neural Network-based Modeling of Snow Properties Using Field Data and Hyperspectral Imagery." *Natural Resource Modeling* 32 (4): 530.
- He, G., X. Feng, P. Xiao, Z. Xia, Z. Wang, H. Chen, H. Li, and J. Guo. 2017. "Dry and Wet Snow Cover Mapping in Mountain Areas Using SAR and Optical Remote Sensing Data." *IEEE J Sel Top Appl Earth Obs Remote Sens* 10 (6): 2575–2588.
- Holden, M., A. S. Solberg, and R. Solberg 1998. Wet Snow-cover Mapping by C- and L-band Polarimetric SAR. In: Int Geosci Remote Sens Symp., Seattle, WA, Vol. 3.: IEEE; p. 1533–1537.
- Hou, J., C. Huang, Y. Zhang, J. Guo, and J. Gu. 2019. "Gap-Filling of MODIS Fractional Snow Cover Products via Non-Local Spatio-Temporal Filtering Based on Machine Learning Techniques." *Remote Sensing* 11 (1): 90. <https://www.mdpi.com/2072-4292/11/1/90>.
- Iru, R., T. Nagler, H. Rott, and G. Glendinning. 1998. "SAR-based Snow Cover Retrievals for Runoff Modelling." *Orbit An Int J Orbital Disord Facial Reconstr Surg* 441: 511–518. November. <http://esamultimedia.esa.int/conferences/98c07/papers/P013.PDF>
- Jeelani, G., J. J. Feddema, C. J. van der Veen, and L. Stearns. 2012. "Role of Snow and Glacier Melt in Controlling River Hydrology in Liddar Watershed (Western Himalaya) under Current and Future Climate." *Water Resources Research* 48 (12). <http://doi.wiley.com/10.1029/2011WR011590>.
- Jiang, Q. 2003. "Moist Dynamics and Orographic Precipitation." *Tellus A Dyn Meteorol Oceanogr* 55 (4): 301–316. <https://www.tandfonline.com/action/journalInformation?journalCode=zela20>.
- Johnston, R., and V. Smakhtin. 2014. "Hydrological Modeling of Large River Basins: How Much Is Enough?" *Water Resour Manag* 28 (10): 2695–2730.
- Joshi, R., K. Kumar, J. Pandit, and L. M. S. Palni. 2015. *Variations in the Seasonal Snow Cover Area (SCA) for Upper Bhagirathi Basin, India*, 9–21. Cham: Springer.
- Karbou, F., G. Veyssiére, C. Coleou, A. Dufour, I. Gouttevin, P. Durand, S. Gascoin, and M. Grizonnet. 2021. "Monitoring Wet Snow over an Alpine Region Using Sentinel-1 Observations." *Remote Sensing* 13 (3): 1–22. doi:[10.3390/rs13030381](https://doi.org/10.3390/rs13030381).
- Kendra, J. R., F. T. Ulaby, and K. Sarabandi. 1994. "Snow Probe for in Situ Determination of Wetness and Density." *IEEE Transactions on Geoscience and Remote Sensing : A Publication of the IEEE Geoscience and Remote Sensing Society* 32 (6): 1152–1159.
- Kinar, N. J., and J. W. Pomeroy. 2015. "Measurement of the Physical Properties of the Snowpack." *Rev Geophys* 53 (2): 481–544.
- Kirkham, J. D., I. Koch, T. M. Saloranta, M. Litt, E. E. Stigter, K. Møen, A. Thapa, K. Melvold, and W. W. Immerzeel. 2019. "Near Real-Time Measurement of Snow Water Equivalent in the Nepal Himalayas." *Front Earth Sci* 7: 177. <https://www.frontiersin.org/article/10.3389/feart.2019.00177/full>.
- Koike, T., and T. Suhama. 1993. "Passive-microwave Remote Sensing of Snow." *Annals of Glaciology*, no. 18: 305–308. <https://www.cambridge.org/core>.
- Kokhanovsky, A. A., and E. P. Zege. 2004. "Scattering Optics of Snow." *Applied Optics* 43 (7): 1589–1602. <https://www.osapublishing.org/viewmedia.cfm?uri=ao-43-7-1589&seq=0&html=true>.
- Kontu, A., S. Leinss, H. Löwe, and M. Proksch. 2020. "Modeling the Evolution of the Structural Anisotropy of Snow." *Cryosphere* 14 (1): 51–75.
- Kulkarni, A. V., S. K. Singh, P. Mathur, and V. D. Mishra. 2006. "Algorithm to Monitor Snow Cover Using AWIFS Data of RESOURCESAT-1 for the Himalayan Region." *International Journal of Remote Sensing* 27 (12): 2449–2457. <https://www.tandfonline.com/doi/full/10.1080/01431160500497820>.
- Kunzi, K. F., S. Patil, and H. Rott. 1982. "Snow-Cover Parameters Retrieved from Nimbus-7 Scanning Multichannel Microwave Radiometer (SMMR) Data." *IEEE Transactions on Geoscience and Remote Sensing : A Publication of the IEEE Geoscience and Remote Sensing Society* GE-20 (4): 452–467.
- Kuter, S., Z. Akyurek, and G. W. Weber. 2018. "Retrieval of Fractional Snow Covered Area from MODIS Data by Multivariate Adaptive Regression Splines." *Remote Sensing of Environment* 205: 236–252.
- Lampkin, D. J., and S. R. Yool. 2004. "Monitoring Mountain Snowpack Evolution Using Near-surface Optical and Thermal Properties." *Hydrological Processes* 18 (18): 3527–3542.
- Lee, K. S., D. Jin, J. M. Yeom, M. Seo, S. Choi, J. J. Kim, and K. S. Han. 2017. "New Approach for Snow Cover Detection through Spectral Pattern Recognition with MODIS Data." *Journal of Sensors* 2017:15. doi:[10.1155/2017/4820905](https://doi.org/10.1155/2017/4820905)
- Leinß, S., and I. Hajnsek. 2012. *Opportunities of Snow Property Extraction Based on Single and Multi Pass SAR Interferometry: TanDEM-X*, Int Geosci Remote Sens Symp. IEEE, 146–149.

- Leinss, S., G. Parrella, and I. Hajnsek. 2014. "Snow Height Determination by Polarimetric Phase Differences in X-Band SAR Data." *IEEE Journal of Selected Topics in Applied Earth Observations and Remote Sensing* 7 (9): 3794–3810.
- Leinss, S., H. Löwe, M. Proksch, J. Lemmettyinen, A. Wiesmann, and I. Hajnsek. 2016. Anisotropy of Seasonal Snow Measured by Polarimetric Phase Differences in Radar Time Series. 1771–1797.
- Leroux, C., and M. Fily. 1998. "Modeling the Effect of Sastrugi on Snow Reflectance." *J Geophys Res Planets* 103 (E11): 25779–25788. <https://agupubs.onlinelibrary.wiley.com/doi/abs/10.1029/98JE00558>.
- Li, H., X. Li, D. Yang, J. Wang, B. Gao, X. Pan, Y. Zhang, and X. Hao. 2019. "Tracing Snowmelt Paths in an Integrated Hydrological Model for Understanding Seasonal Snowmelt Contribution at Basin Scale." *J Geophys Res Atmos* 124 (16): 8874–8895. <https://onlinelibrary.wiley.com/doi/abs/10.1029/2019JD030760>.
- Li, H., Z. Wang, G. He, and W. Man. 2017. "Estimating Snow Depth and Snow Water Equivalence Using Repeat-Pass Interferometric SAR in the Northern Piedmont Region of the Tianshan Mountains." *Journal of Sensors* 2017: 1–17.
- Liang, J., X. Liu, K. Huang, X. Li, X. Shi, Y. Chen, and J. Li. 2015. "Improved Snow Depth Retrieval by Integrating Microwave Brightness Temperature and Visible/infrared Reflectance." *Remote Sensing of Environment* 156: 500–509.
- Lievens, H., M. Demuzere, H. P. Marshall, R. H. Reichle, L. Brucker, I. Brangers, P. De Rosnay, et al. 2019. "Snow Depth Variability in the Northern Hemisphere Mountains Observed from Space." *Nature Communications* 10 (1): 1–12. doi:10.1038/s41467-019-12566-y.
- Liu, Y., L. Li, J. Yang, X. Chen, and J. Hao. 2017. "Estimating Snow Depth Using Multi-source Data Fusion Based on the D-InSAR Method and 3DVAR Fusion Algorithm." *Remote Sensing* 9: 11.
- Looyenga, H. 1965. "Dielectric Constants of Heterogeneous Mixtures." *Physica* 31 (3): 401–406. <https://www.sciencedirect.com/science/article/pii/0031891465900455>.
- Luojuus, K. P., J. T. Pulliaainen, S. J. Metsämäki, and M. T. Hallikainen. 2007. "Snow-covered Area Estimation Using Satellite Radar Wide-swath Images." *IEEE Transactions on Geoscience and Remote Sensing : A Publication of the IEEE Geoscience and Remote Sensing Society* 45 (4): 978–988.
- Mahmoodzada, A. B., D. Varade, and S. Shimada. 2020. "Estimation of Snow Depth in the Hindu Kush Himalayas of Afghanistan during Peak Winter and Early Melt Season." *Remote Sensing* 12 (17): 2788. <https://www.mdpi.com/2072-4292/12/17/2788>.
- Malnes, E., and T. Guneriusson. 2002. "Mapping of Snow Covered Area with Radarsat in Norway." *International Geoscience and Remote Sensing Symposium* 1.: 683–685.
- Manickam, S., A. Bhattacharya, G. Singh, and Y. Yamaguchi. 2016. "Estimation of Snow Surface Dielectric Constant from Polarimetric SAR Data." *IEEE J Sel Top Appl Earth Obs Remote Sens* 10 (1): 211–218.
- Marshall, G. J., J. A. Dowdeswell, and W. G. Rees. 1994. "The Spatial and Temporal Effect of Cloud Cover on the Acquisition of High Quality Landsat Imagery in the European Arctic Sector." *Remote Sensing of Environment* 50 (2): 149–160.
- Marti, R., S. Gascoin, E. Berthier, M. De Pinel, T. Houet, and D. Laffly. 2016. "Mapping Snow Depth in Open Alpine Terrain from Stereo Satellite Imagery." *Cryosphere* 10 (4): 1361–1380.
- Maslanka, W., M. Sandells, R. Gurney, J. Lemmettyinen, L. Leppanen, A. Kontu, M. Matzl, N. Rutter, T. Watts, and R. Kelly. 2019. "Derivation and Evaluation of a New Extinction Coefficient for Use with the n-HUT Snow Emission Model." *IEEE Transactions on Geoscience and Remote Sensing : A Publication of the IEEE Geoscience and Remote Sensing Society* 57 (10): 7406–7417.
- Masson, T., M. Dumont, M. Mura, P. Sirguey, S. Gascoin, and C. J. Dedieu J.-P. 2018. "An Assessment of Existing Methodologies to Retrieve Snow Cover Fraction from MODIS Data." *Remote Sensing* 10 (4): 619. <http://www.mdpi.com/2072-4292/10/4/619>.
- Mätzler, C. 1994. "Passive Microwave Signatures of Landscapes in Winter." *Meteorology and Atmospheric Physics* 54 (1–4): 241–260.
- Mätzler, C. 1996. "Microwave Permittivity of Dry Snow." *IEEE Transactions on Geoscience and Remote Sensing : A Publication of the IEEE Geoscience and Remote Sensing Society* 34 (2): 573–581.
- Mätzler, C. 2006. Thermal Microwave Radiation: Applications for Remote Sensing: let.
- Matzler, C., T. Strozzi, T. Weise, D. M. Floricioiu, and H. Rott. 1997. "Microwave Snowpack Studies Made in the Austrian Alps during the SIR-C/X-SAR Experiment." *International Journal of Remote Sensing* 18 (12): 2505–2530. <https://www.tandfonline.com/doi/abs/10.1080/014311697217440>.
- McGregor, G. R. 1990. "Snowpack Structure and Avalanching, Craigieburn Range, New Zealand." *New Zeal J Geol Geophys* 33 (3): 405–471. doi:10.1080/00288306.1990.10425697.
- Meløysund, V., B. Leira, K. V. Høiseth, and K. R. Lisø. 2007. "Predicting Snow Density Using Meteorological Data." *Meteorol Appl* 14 (4): 413–423.
- Mithen, S., and E. Black. 2011. "Overview and Reflections: 20,000 Years of Water and Human Settlement in the Southern Levant." *Water, Life Civilis Clim Environ Soc Jordan* (2011): 469–480.
- Montpetit, B., A. Royer, A. Roy, A. Langlois, and C. Derkisen. 2013. "Snow Microwave Emission Modeling of Ice Lenses within a Snowpack Using the Microwave Emission Model for Layered Snowpacks." *IEEE Transactions on Geoscience and Remote Sensing : A Publication of the IEEE Geoscience and Remote Sensing Society* 51 (9): 4705–4717.
- Muhuri, A., D. Ratha, and A. Bhattacharya. 2017. "Seasonal Snow Cover Change Detection over the Indian Himalayas Using Polarimetric SAR Images." *IEEE Geoscience and Remote Sensing Letters* 14 (12): 2340–2344.
- Muhuri, A., S. Manickam, A. Bhattacharya, and Snehamini. 2018. "Snow Cover Mapping Using Polarization Fraction Variation with Temporal RADARSAT-2 C-Band Full-Polarimetric SAR Data over the Indian Himalayas." *IEEE J Sel Top Appl Earth Obs Remote Sens* 11 (7): 2192–2209.

- Nagler, T. 1991. *Nagler, T (1991). Verfahren zur Analyse der Schneedeckung aus Messungen des SSM/I.* Innsbruck, Austria: University of Innsbruck.
- Nagler, T. 1996. Methods and Analysis of Synthetic Aperture Radar Data from ERS-1 and X-SAR for Snow and Glacier Applications: Verlag Nicht Ermittelbar. <https://books.google.co.in/books?id=aiypmQEACAAJ>
- Nagler, T., and H. Rott. 2000. "Retrieval of Wet Snow by Means of Multitemporal SAR Data." *IEEE Transactions on Geoscience and Remote Sensing : A Publication of the IEEE Geoscience and Remote Sensing Society* 38 (2 I): 754–765.
- Nagler, T., H. Rott, E. Ripper, G. Bippus, and M. Hetzenegger. 2016. "Advancements for Snowmelt Monitoring by Means of Sentinel-1 SAR." *Remote Sensing* 8 (4): 348.
- Nagler, T., H. Rott, and G. Glendinning. 2000. "Snowmelt Runoff Modelling by Means of Radarsat and Ers Sar." *Can J Remote Sens* 26 (6): 512–520.
- Nagler, T., H. Rott, P. Malcher, and F. Müller. 2008. "Assimilation of Meteorological and Remote Sensing Data for Snowmelt Runoff Forecasting." *Remote Sensing of Environment* 112 (4): 1408–1420.
- Najibi, N., and S. Jin. 2013. "Physical Reflectivity and Polarization Characteristics for Snow and Ice-Covered Surfaces Interacting with GPS Signals." *Remote Sensing* 5 (8): 4006–4030. <http://www.mdpi.com/2072-4292/5/8/4006>.
- Negi, H. S., and A. Kokhanovsky. 2011. "Retrieval of Snow Grain Size and Albedo of Western Himalayan Snow Cover Using Satellite Data." *Cryosph* 5 (4): 831–847.
- Negi, H. S., H. S. Jassar, G. Saravana, N. K. Thakur, and G. A. Snehrmani. 2013. "Snow-cover Characteristics Using Hyperion Data for the Himalayan Region." *Int J Remote Sensing* 34 (6): 2140–2161. <https://www.tandfonline.com/doi/full/10.1080/01431161.2012.742213>.
- Nolin, A. W., and J. Dozier. 2000. "A Hyperspectral Method for Remotely Sensing the Grain Size of Snow." *Remote Sensing of Environment* 74 (2): 207–216.
- Nolin, A. W., J. Dozier, and L. A. K. Mertes. 1993. "Mapping Alpine Snow Using a Spectral Mixture Modeling Technique." *Annals of Glaciology* 17: 121–124. <https://www.cambridge.org/core>.
- Notarnicola, C., R. Ratti, V. Maddalena, T. Schellenberger, B. Ventura, and M. Zebisch. 2013. "Seasonal Snow Cover Mapping in Alpine Areas through Time Series of COSMO-skymed Images." *IEEE Geoscience and Remote Sensing Letters* 10 (4): 716–720.
- Ostrem, G., N. Haakensen, and R. Eriksson. 1981. "The Glaciation Level in Southern Alaska." *Geogr Ann Ser A* 63 (3–4): 251–260. <https://www.tandfonline.com/doi/abs/10.1080/04353676.1981.11880040>.
- Painter, T. H., J. Dozier, D. A. Roberts, R. E. Davis, and R. O. Green. 2003. "Retrieval of Subpixel Snow-covered Area and Grain Size from Imaging Spectrometer Data." *Remote Sensing of Environment* 85 (1): 64–77.
- Pardé, M., K. Goita, and A. Royer. 2007. "Inversion of a Passive Microwave Snow Emission Model for Water Equivalent Estimation Using Airborne and Satellite Data." *Remote Sensing of Environment* 111 (2–3): 346–356.
- Patil, A., S. Mohanty, and G. Singh. 2020. "Snow Depth and Snow Water Equivalent Retrieval Using X-band PolInSAR Data." *Remote Sensing Letters* 11 (9): 817–826. doi:[10.1080/2150704X.2020.1779373](https://doi.org/10.1080/2150704X.2020.1779373)
- Patil, A., G. Singh, and C. Rüdiger. 2020. "Retrieval of Snow Depth and Snow Water Equivalent Using Dual Polarization SAR Data." *Remote Sensing* 12 (7): 1183. <https://www.mdpi.com/2072-4292/12/7/1183>.
- Patil, A., S. Mohanty, and G. Singh. 2020. "Snow Depth and Snow Water Equivalent Retrieval Using X-band PolInSAR Data." *Remote Sensing Letters* 11 (9): 817–826. doi:[10.1080/2150704X.2020.1779373](https://doi.org/10.1080/2150704X.2020.1779373).
- Pepe, M., P. A. Brivio, A. Rampini, F. R. Nodari, and M. Boschetti. 2005. "Snow Cover Monitoring in Alpine Regions Using ENVISAT Optical Data." *International Journal of Remote Sensing* 26 (21): 4661–4667.
- Pielmeier, C., and M. Schneebeli. 2003. "Developments in the Stratigraphy of Snow." *Surv Geophys* 24 (5/6): 389–416.
- Pomeroy, J. W. 2007. "Cold Regions Hydrology, Snow, and PUB." In Predict Ungauged Basins: PUB Kick-off. 85–91. Wallingford, UK: IAHS Press.
- Pottier, E., and J.-S. Lee. 2009. *Polarimetric Radar Imaging*. Boca Raton, Florida: CRC Press.
- Poussin, C., Y. Guigoz, E. Palazzi, S. Terzago, B. Chatenoux, and G. Giuliani. 2019. "Snow Cover Evolution in the Gran Paradiso National Park, Italian Alps, Using the Earth Observation Data Cube." *Data* 4 (4): 138. <https://www.mdpi.com/2306-5729/4/4/138>.
- Pütz, M., D. Gallati, S. Kyttia, H. Elsasser, C. Lardelli, M. Teich, F. Waltert, and C. Rixen. 2011. "Winter Tourism, Climate Change, and Snowmaking in the Swiss Alps: Tourists' Attitudes and Regional Economic Impacts." *Mountain Research and Development* 31 (4): 357–362.
- Rango, A. 1993. "II. Snow Hydrology Processes and Remote Sensing." *Hydrological Processes* 7 (2): 121–138. doi:[10.1002/hyp.3360070204](https://doi.org/10.1002/hyp.3360070204).
- Rao, Y. S., G. Venkataraman, and G. Singh. 2006. "ENVISAT-ASAR Data Analysis for Snow Cover Mapping over Gangotri Region." *IProc. SPIE* 6410, Microwave Remote Sensing of the Atmosphere and Environment V, 641007 (7 December 2006): 641007. doi:[10.1117/12.693845](https://doi.org/10.1117/12.693845)
- Riche, F., M. Montagnat, and M. Schneebeli. 2013. "Evolution of Crystal Orientation in Snow during Temperature Gradient Metamorphism." *Journal of Glaciology* 59 (213): 47–55. <https://www.cambridge.org/core>.
- Rittger, K., M. S. Raleigh, J. Dozier, A. F. Hill, J. A. Lutz, and T. H. Painter. 2020. "Canopy Adjustment and Improved Cloud Detection for Remotely Sensed Snow Cover Mapping." *Water Resources Research* 56 (6). <https://agu-pubs.onlinelibrary.wiley.com/doi/full/10.1029/2019WR024914>.
- Rott, H., T. Nagler, and R. Scheiber. 2004. "Snow Mass Retrieval by Means of Sar Interferometry." *European Space Agency* 2003 (550): 187–192.

- Saberi, N., R. Kelly, M. Flemming, and Q. Li. 2020. "Review of Snow Water Equivalent Retrieval Methods Using Spaceborne Passive Microwave Radiometry." *International Journal of Remote Sensing* 41 (3): 996–1018. <https://www.tandfonline.com/action/journalInformation?journalCode=tres20>.
- Sadeghi, M., E. Babaeian, M. Tuller, and S. B. Jones. 2017. "The Optical Trapezoid Model: A Novel Approach to Remote Sensing of Soil Moisture Applied to Sentinel-2 and Landsat-8 Observations." *Remote Sensing of Environment* 198: 52–68.
- Saito, A., and T. Yamazaki. 1999. "Characteristics of Spectral Reflectance for Vegetation Ground Surfaces with Snow-cover; Vegetation Indices and Snow Indices." *J Japan Soc Hydrol Water Resour* 12 (1): 28–38.
- Shao, D., H. Li, J. Wang, X. Pan, and X. Hao. 2017. "Distinguishing the Role of Wind in Snow Distribution by Utilizing Remote Sensing and Modeling Data: Case Study in the Northeastern Tibetan Plateau." *IEEE J Sel Top Appl Earth Obs Remote Sens* 10 (10): 4445–4456.
- Sharma, R. C., R. Tateishi, and K. Hara. 2016. "A New Water-resistant Snow Index for the Detection and Mapping of Snow Cover on A Global Scale." *International Journal of Remote Sensing* 37 (11): 2706–2723. <https://www.tandfonline.com/doi/full/10.1080/01431161.2016.1183832>.
- Shaw, T. E., C. Deschamps-Berger, S. Gascoin, and J. McPhee. 2020a. "Monitoring Spatial and Temporal Differences in Andean Snow Depth Derived from Satellite Tri-Stereo Photogrammetry." *Front Earth Sci* 8 (December): 1–16.
- Shaw, T. E., S. Gascoin, P. A. Mendoza, F. Pellicciotti, and J. McPhee. 2020b. "Snow Depth Patterns in a High Mountain Andean Catchment from Satellite Optical Tristereoscopic Remote Sensing." *Water Resources Research* 56 (2): 1–23.
- Shekhar, C., S. Srivastava, H. S. Negi, and M. Dwivedi. 2019. "Hyper-spectral Data Based Investigations for Snow Wetness Mapping." *Geocarto International* 34 (6): 664–687. <https://www.tandfonline.com/doi/full/10.1080/10106049.2018.1438528>.
- Shi, J. 2006. "Snow Water Equivalence Retrieval Using X and Ku Band Dual-polarization Radar." In *IEEE International Geoscience and Remote Sensing* 2183–2185.
- Shi, J., and J. Dozier. 1995. "Inferring Snow Wetness Using C-Band Data from SIR-C's Polarimetric Synthetic Aperture Radar." *IEEE Transactions on Geoscience and Remote Sensing : A Publication of the IEEE Geoscience and Remote Sensing Society* 33 (4): 905–914.
- Shi, J., and J. Dozier. 1997. "Mapping Seasonal Snow with SIR-C/X-SAR in Mountainous Areas." *Remote Sensing of Environment* 59 (2): 294–307.
- Shi, J., and J. Dozier. 2000a. "Estimation of Snow Water Equivalence Using SIR-C/X-SAR, Part I: Inferring Snow Density and Subsurface Properties." *IEEE Transactions on Geoscience and Remote Sensing : A Publication of the IEEE Geoscience and Remote Sensing Society* 38 (6): 2465–2474.
- Shi, J., and J. Dozier. 2000b. "Estimation of Snow Water Equivalence Using SIR-C/X-SAR, Part II: Inferring Snow Depth and Particle Size." *IEEE Transactions on Geoscience and Remote Sensing : A Publication of the IEEE Geoscience and Remote Sensing Society* 38 (6): 2475–2488.
- Shi, J., S. Hensley, and J. Dozier. 2000. "Mapping Snow with Repeat Pass Synthetic Aperture Radar." *Geosci Remote Sensing, 1997 IGARSS '97 Remote Sens - A Sci Vis Sustain Dev 1997 IEEE Int* 2000 (267): 339–342.
- Shi, J. C., C. Xiong, and L. M. Jiang. 2016. "Review of Snow Water Equivalent Microwave Remote Sensing." *Sci China Earth Sci* 59 (4): 731–745. <https://link.springer.com/article/10.1007/s11430-015-5225-0>.
- Sihvola, A., and M. Tiuri. 1986. "Snow Fork for Field Determination of the Density and Wetness Profiles of a Snow Pack." *IEEE Transactions on Geoscience and Remote Sensing : A Publication of the IEEE Geoscience and Remote Sensing Society* GE-24 (5): 717–721.
- Siler, N., and G. Roe. 2014. "How Will Orographic Precipitation Respond to Surface Warming? An Idealized Thermodynamic Perspective." *Geophysical Research Letters* 41 (7): 2606–2613. doi:10.1002/2013GL059095.
- Singh, G., V. Kumar, K. Mohite, G. Venkataraman, Y. S. Rao, and Snehmani. 2006. "Snow Wetness Estimation in Himalayan Snow Covered Regions Using ENVISAT-ASAR Data." In *Microw Remote Sens Atmos Environ V*. Vol. 6410: 641008. doi:10.1117/12.693690.
- Singh, G., A. Verma, S. Kumar, G. A. Snehmani, Y. Yamaguchi, and A. V. Kulkarni. 2017. "Snowpack Density Retrieval Using Fully Polarimetric TerraSAR-X Data in the Himalayas." *IEEE Trans Geosci Remote Sensing* 55 (11): 6320–6329. <http://ieeexplore.ieee.org/document/8000412/>
- Singh, G., and G. Venkataraman. 2010. "Snow Permittivity Retrieval Inversion Algorithm for Estimating Snow Wetness." *Geocarto International* 25 (3): 187–212. <https://www.tandfonline.com/doi/abs/10.1080/10106040903486130>.
- Singh, G., G. Venkataraman, Y. Yamaguchi, and S. E. Park. 2014. "Capability Assessment of Fully Polarimetric Alos-palsar Data for Discriminating Wet Snow from Other Scattering Types in Mountainous Regions." *IEEE Transactions on Geoscience and Remote Sensing : A Publication of the IEEE Geoscience and Remote Sensing Society* 52 (2): 1177–1196.
- Singh, G., G. Venkataraman, Y. S. Rao, V. Kumar, and Snehmani. 2008. "The H/A/ALPHA Polarimetric Decomposition Theorem and Complex Wishart Distribution for Snow Cover Monitoring." *International Geoscience and Remote Sensing Symposium* 4: IV-1081.
- Singh, P., K. S. Ramasastri, and N. Kumar. 1995. "Topographical Influence on Precipitation Distribution in Different Ranges of Western Himalayas." *Hydrol Res* 26 (4–5): 259–284.
- Singh, S., V. Sood, R. Kaur, and S. Prashar. 2019. "An Efficient Algorithm for Detection of Seasonal Snow Cover Variations over Undulating North Indian Himalayas, India." *Adv Sp Res* 64 (2): 314–327.
- Singh, V. P., P. Singh, and U. K. Haritashya. 2011. *Encyclopedia of Snow, Ice and Glaciers*. Dordrecht: Springer Netherlands.
- Sniper, B., A. Momblanch, S. K. Jain, T. W. Waine, and I. P. Holman. 2019. "A Method for Monthly Mapping of Wet

- and Dry Snow Using Sentinel-1 and MODIS: Application to A Himalayan River Basin." *International Journal of Applied Earth Observation and Geoinformation : ITC Journal* 74: 222–230.
- Snehmani, S. M. K., R. D. Gupta, A. Bhardwaj, and P. K. Joshi. 2015. "Remote Sensing of Mountain Snow Using Active Microwave Sensors: A Review." *Geocarto International* 30 (1): 1–27. <http://www.tandfonline.com/doi/abs/10.1080/10106049.2014.883434>
- Snehmani, V. G., A. K. Nigam, and G. Singh. 2010. "Development of an Inversion Algorithm for Dry Snow Density Estimation and Its Application with ENVISAT-ASAR Dual Co-polarization Data." *Geocarto International* 25 (8): 597–616. <http://www.tandfonline.com/doi/abs/10.1080/10106049.2010.516843>
- Snow and Climate | National Snow and Ice Data Center. [accessed 2021 May 7]. <https://nsidc.org/cryosphere/snow/climate.html>
- Snyder, W. 1997. "Thermal Infrared Bidirectional Reflectance Measurements of Sands and Soils." *Remote Sensing of Environment* 60 (1): 101–109.
- Sommerfeld, R. A., and E. LaChapelle. 1970. "The Classification of Snow Metamorphism." *Journal of Glaciology* 9 (55): 3–18.
- Steinkogler, W., B. Sovilla, and M. Lehning. 2014. "Influence of Snow Cover Properties on Avalanche Dynamics." *Cold Regions Science and Technology* 97: 121–131.
- Stiles, W. H., and F. T. Ulaby. 1981. Dielectric Properties of Snow. 49–71.
- Stiles, W. H., F. T. Ulaby, and A. Rango. 1981. "Microwave Measurements of Snowpack Properties." *Nord Hydrol* 12 (3): 143–166.
- Storvold, R., and E. Malnes. 2004. "Snow Covered Area Retrieval Using ENVISAT ASAR Wideswath in Mountainous Areas." *International Geoscience and Remote Sensing Symposium* 3: 1845–1848.
- Strozzi, T., A. Wiesmann, and C. Mätzler. 1997. "Active Microwave Signatures of Snow Covers at 5.3 And 35 GHz." *Radio Sci* 32 (2): 479–495.
- Strozzi, T., U. Wegmuller, and C. Matzler. 1999. "Mapping Wet Snowcovers with SAR Interferometry." *International Journal of Remote Sensing* 20 (12): 2395–2403. <https://www.tandfonline.com/doi/abs/10.1080/014311699212083>
- Surendar, M., A. Bhattacharya, G. Singh, and G. Venkataraman. 2015. "Estimation of Snow Density Using Full-polarimetric Synthetic Aperture Radar (SAR) Data." *Phys Chem Earth* 83–84: 156–165. Parts A/B/C. <https://www.sciencedirect.com/science/article/pii/S1474706515000741>
- Techel, F., and C. Pielmeier. 2011. "Point Observations of Liquid Water Content in Wet Snow - Investigating Methodical, Spatial and Temporal Aspects." *Cryosph* 5 (2): 405–418.
- Tedesco, M., J. Pulliainen, M. Takala, M. Hallikainen, and P. Pampaloni. 2004. "Artificial Neural Network-based Techniques for the Retrieval of SWE and Snow Depth from SSM/I Data." *Remote Sensing of Environment* 90 (1): 76–85.
- Tekeli, A. E., I. Sönmez, and E. Erdi. 2016. "Snow-covered Area Determination Based on Satellite-derived Probabilistic Snow Cover Maps." *Arabian Journal of Geosciences* 9 (3): 1–11. <https://link.springer.com/article/10.1007/s12517-015-2149-0>.
- Thakur, P. K., R. D. Garg, S. P. Aggarwal, P. K. Garg, and S. J. Snehmani. 2013. "Snow Density Retrieval Using SAR Data: Algorithm Validation and Applications in Part of North Western Himalaya." *Cryosph Discuss* 7 (3): 1927–1960. <http://www.the-cryosphere-discuss.net/7/1927/2013/>.
- Thakur, P. K., S. P. Aggarwal, G. Arun, S. Sood, A. Senthil Kumar, S. Mani, and D. P. Dobhal. 2016. "Estimation of Snow Cover Area, Snow Physical Properties and Glacier Classification in Parts of Western Himalayas Using C-Band SAR Data." *J Indian Soc Remote* 45 (3): 1–15.
- Thakur, P. K., S. P. Aggarwal, P. K. Garg, R. D. Garg, S. Mani, S. Kumar, K. Thakur Praveen, et al. 2012. "Snow Physical Parameters Estimation Using Space- Based Synthetic Aperture Radar." *Geocarto International* 6049 (August): 2016.
- Tiuri, M. E., A. H. Sihvola, E. G. Nyfors, and M. T. Hallikainen. 1984. "The Complex Dielectric Constant of Snow at Microwave Frequencies." *IEEE Journal of Oceanic Engineering* 9 (5): 377–382.
- Töglhofer, C., F. Eigner, and F. Prettenthaler. 2011. "Impacts of Snow Conditions on Tourism Demand in Austrian Ski Areas." *Clim Res* 46 (1): 1–14. <http://www.int-res.com/abstracts/cr/v46/n1/p1-14/>.
- Treichler, D., and A. Kääb. 2017. "Snow Depth from ICESat Laser Altimetry — A Test Study in Southern Norway." *Remote Sensing of Environment* 191: 389–401.
- Tsai, Y.-L. S., A. Dietz, N. Oppelt, and C. Kuenzer. 2019. "Remote Sensing of Snow Cover Using Spaceborne SAR: A Review." *Remote Sensing* 11 (12): 1456.
- Tsang, L., D. Liang, X. Xu, and P. Xu. 2008. Microwave Emission from Snowpacks: Modeling the Effects of Volume Scattering, Surface Scattering and Layering. In: 2008 Microw Radiom Remote Sens Environ - 10th Spec Meet Proceedings, MICRORAD, Florence, Italy .
- Tsang, L., S. Tan, X. Xu, and K. H. Ding. 2016. Scattering and Emission Models for Microwave Remote Sensing of Snow Using Numerical Solutions of Maxwell Equations. In: Int Geosci Remote Sens Symp. Vol. 2016-Nov Institute of Electrical and Electronics Engineers, Beijing, China ; p. 7050–7052.
- Tsang, L., Z. Chen, S. Oh, R. J. Marks, and A. T. C. Chang. 1992. "Inversion of Snow Parameters from Passive Microwave Remote Sensing Measurements by a Neural Network Trained with a Multiple Scattering Model." *IEEE Transactions on Geoscience and Remote Sensing : A Publication of the IEEE Geoscience and Remote Sensing Society* 30 (5): 1015–1024.
- Tse, K. K., L. Tsang, C. H. Chan, K. H. Ding, and K. W. Leung. 2007. "Multiple Scattering of Waves by Dense Random Distributions of Sticky Particles for Applications in Microwave Scattering by Terrestrial Snow." *Radio Science* 42 (5). doi:[10.1029/2006RS003476](https://doi.org/10.1029/2006RS003476).
- Ulaby, F. T., D. G. Long, W. J. Blackwell, C. Elachi, A. K. Fung, C. Ruf, K. Sarabandi, H. A. Zebker, and J. Van Zyl. 2014.

- Microwave Radar and Radiometric Remote Sensing.* Ann Arbor: University of Michigan Press.
- Ulaby, F. T., F. Kouyate, A. K. Fung, and A. J. Sieber. 1982. "A Backscatter Model for A Randomly Perturbed Periodic Surface." *IEEE Transactions on Geoscience and Remote Sensing : A Publication of the IEEE Geoscience and Remote Sensing Society* GE-20 (4): 518–528.
- Ulaby, F. T., R. K. Moore, and A. K. Fung 1981. *Microwave Remote Sensing: Active and Passive*: Artech House. <https://books.google.co.in/books?id=sZB5wwEACAAJ>
- Ulaby, F. T., W. H. Stiles, L. F. Dellwig, and B. C. Hanson. 1977. "Experiments on the Radar Backscatter of Snow." *Geosci Electron IEEE Trans* 15 (4): 185–189.
- Usami, N., A. Muhuri, A. Bhattacharya, and A. Hirose. 2016. "Proposal of Wet Snowmapping with Focus on Incident Angle Influential to Depolarization of Surface Scattering." In *IEEE International Geoscience and Remote Sensing Symposium* 1544–1547. 2016-Nov.
- Vander Jagt, B., A. Lucieer, L. Wallace, D. Turner, and M. Durand. 2015. "Snow Depth Retrieval with UAS Using Photogrammetric Techniques." *Geosciences* 5 (3): 264–285.
- Vanonckelen, S., S. Lhermitte, and A. Van Rompaey. 2013. "The Effect of Atmospheric and Topographic Correction Methods on Land Cover Classification Accuracy." *International Journal of Applied Earth Observation and Geoinformation : ITC Journal* 24 (1): 9–21.
- Varade, D., A. Sure, and O. Dikshit. 2019. "Potential of Landsat-8 and Sentinel-2A Composite for Land Use Land Cover Analysis." *Geocarto International* 34 (14): 1552–1567. <https://www.tandfonline.com/doi/full/10.1080/10106049.2018.1497096>
- Varade, D., A. K. Maurya, A. Sure, and O. Dikshit 2018a. „Supervised Classification of Snow Cover Using Hyperspectral Imagery." In: 2017 Int Conf Emerg Trends Comput Commun Technol ICETCCT 2017. Vol. 2018, Dehradun, India. Institute of Electrical and Electronics Engineers ; p. 1–7.
- Varade, D., A. K. Maurya, and O. Dikshit 2019a. Unsupervised Band Selection of Hyperspectral Data Based on Mutual Information Derived from Weighted Cluster Entropy for Snow Classification. *Geocarto International*. 1–23. <https://www.tandfonline.com/doi/full/10.1080/10106049.2019.1665717>
- Varade, D., A. K. Maurya, O. Dikshit, G. Singh, and S. Manickam. 2020b. "Snow Depth in Dhundi: An Estimate Based on Weighted Bias Corrected Differential Phase Observations of Dual Polarimetric Bi-temporal Sentinel-1 Data." *International Journal of Remote Sensing* 41 (8): 3031–3053.
- Varade, D., G. Singh, O. Dikshit, and S. Manickam. 2020c. "Identification of Snow Using Fully Polarimetric SAR Data BVarade D, Singh G, Dikshit O, Manickam S. 2020." *Water Resources Research* 56: 2. <https://onlinelibrary.wiley.com/doi/abs/10.1029/2019WR025449>.
- Varade, D., and O. Dikshit. 2018. "Estimation of Surface Snow Wetness Using Sentinel-2 Multispectral Data." *ISPRS Ann Photogramm Remote Sens Spat Inf Sci* IV-5: 223–228.
- Varade, D., and O. Dikshit. 2019. "Potential of Multispectral Reflectance for Assessment of Snow Geophysical Parameters in Solang Valley in the Lower Indian Himalayas." *GIScience Remote Sens* 57 (1): 107–126.
- Varade, D., O. Dikshit, and S. Manickam. 2019. "Dry/wet Snow Mapping Based on the Synergistic Use of Dual Polarimetric SAR and Multispectral Data." *J Mt Science* 16 (6): 1435–1451. doi:10.1007/s11629-019-5373-3.
- Varade, D., S. Manickam, O. Dikshit, G. Singh, and Snehamini. 2020a. "Modelling of Early Winter Snow Density Using Fully Polarimetric C-band SAR Data in the Indian Himalayas." *Remote Sensing of Environment* 240: 111699.
- Varade, D. M., A. K. Maurya, and O. Dikshit. 2019b. "Development of Spectral Indexes in Hyperspectral Imagery for Land Cover Assessment." *IETE Tech Rev* 36 (5): 475–483. <https://www.tandfonline.com/doi/full/10.1080/02564602.2018.1503569>
- Vavrus, S. 2007. "The Role of Terrestrial Snow Cover in the Climate System." *Climate Dynamics* 29 (1): 73–88. <https://link.springer.com/article/10.1007/s00382-007-0226-0>
- Wan, Z., D. Ng, and J. Dozier. 1994. "Spectral Emissivity Measurements of Land-surface Materials and Related Radiative Transfer Simulations." *Adv Sp Res* 14 (3): 91–94.
- Wang, X., J. Wang, T. Che, X. Huang, X. Hao, and H. Li. 2018. "Snow Cover Mapping for Complex Mountainous Forested Environments Based on a Multi-Index Technique." *IEEE J Sel Top Appl Earth Obs Remote Sens* 11 (5): 1433–1441.
- White, G., and A. McCallum. 2018. "Review of Ice and Snow Runway Pavements." *Int J Pavement Res Technol* 11 (3): 311–320.
- Wipf, S., and C. Rixen. 2010. "A Review of Snow Manipulation Experiments in Arctic and Alpine Tundra Ecosystems." *Polar Research* 29 (1): 95–109. doi:10.1111/j.1751-8369.2010.00153.x.
- Xiao, X., T. Zhang, X. Zhong, W. Shao, and X. Li. 2018. "Support Vector Regression Snow-depth Retrieval Algorithm Using Passive Microwave Remote Sensing Data." *Remote Sensing of Environment* 210: 48–64.
- Xie, J., M. Kneubühler, I. Garonna, C. Notarnicola, L. De Gregorio, R. De Jong, B. Chimani, and M. E. Schaepman. 2017. "Altitude-dependent Influence of Snow Cover on Alpine Land Surface Phenology." *J Geophys Res Biogeosciences* 122 (5): 1107–1122. <http://www.alpconv.org/>
- Yao, H., T. Field, C. McConnell, A. Beaton, and A. L. James. 2018. "Comparison of Five Snow Water Equivalent Estimation Methods across Categories." *Hydrological Processes* 32 (12): 1894–1908. doi:10.1002/hyp.13129.
- You, Q., T. Wu, L. Shen, N. Pepin, L. Zhang, Z. Jiang, Z. Wu, S. Kang, and A. AghaKouchak. 2020. "Review of Snow Cover Variation over the Tibetan Plateau and Its Influence on the Broad Climate System." *Earth-Science Rev* 201: 103043.
- Yu, L., T. Liu, and S. Zhang. 2017. "Temporal and Spatial Changes in Snow Cover and the Corresponding Radiative Forcing Analysis in Siberia from the 1970s to the 2010s." *Adv Meteorol* 2017: 1–11.
- Yueh, S., D. Cline, and K. Elder 2008. "Airborne Ku-band Polarimetric Radar Remote Sensing of Terrestrial Snow Cover." In: IEEE Radar Conf RADAR, Rome, Italy 26–30 May 2008: 1–6.

- Yueh, S. H., S. J. Dinardo, A. Akgiray, R. West, D. W. Cline, and K. Elder. 2009. "Airborne Ku-band Polarimetric Radar Remote Sensing of Terrestrial Snow Cover." *IEEE Transactions on Geoscience and Remote Sensing : A Publication of the IEEE Geoscience and Remote Sensing Society* 47 (10): 3347–3364.
- Zhang, X., M. A. Friedl, C. B. Schaaf, A. H. Strahler, J. C. F. Hodges, F. Gao, B. C. Reed, and A. Huete. 2003. "Monitoring Vegetation Phenology Using MODIS." *Remote Sensing of Environment* 84 (3): 471–475.
- Zhang, Y., G. Ma, W. Tian, J. Wang, and S. Chen. 2020. "Threshold-Based Adaptive Gaussian Mixture Model Integration (TA-GMMI) Algorithm for Mapping Snow Cover in Mountainous Terrain." *Computer Modeling in Engineering & Sciences : CMES* 124 (3): 1149–1165.
- Zhao, J., Y. Shi, Y. Huang, and J. Fu. 2015. "Uncertainties of Snow Cover Extraction Caused by the Nature of Topography and Underlying Surface." *J Arid Land* 7 (3): 285–295.
- Zhu, L., Y. Zhang, J. Wang, W. Tian, Q. Liu, G. Ma, X. Kan, and Y. Chu. 2021. "Downscaling Snow Depth Mapping by Fusion of Microwave and Optical Remote-Sensing Data Based on Deep Learning." *Remote Sensing* 13 (4): 584.
- Zhuravleva, T. B., and A. A. Kokhanovsky. 2011. "Influence of Surface Roughness on the Reflective Properties of Snow." *Journal of Quantitative Spectroscopy & Radiative Transfer* 112 (8): 1353–1368.

Appendix A

Table A1. SAR missions applicable in remote sensing applications of snow.

Satellite Sensor	Operating Frequency Band	Operation Period	Temporal Repeatability	Operational Imaging modes Resolution(range x azimuth) Swath covered (km) Polarizations
ALOS-PALSAR 2	L-Band at 1.2 GHz Frequency	2013–Present	14 days	Spotlight mode 1 m × 3 m 25 km Single Polarization Strip-map mode 3, 6 or 10 m 50 Km or 70 km Single, Dual or Quad Polarization ScanSAR mode 100 m or 60 m 350 km or 490 km Single or Dual Polarization
RADARSAT-2	C-band at 5.405 GHz	2007–Present	24 days	Spotlight mode 1 m × 1 m 18 km Single Polarization Ultra-Fine mode 3 m × 3 m 20 km Single Polarization Extra-Fine mode 5 m × 5 m 125 km Single Polarization Multi-Look Fine mode 8 m × 8 m 50 Km Single Polarization Fine Quad-Pol mode 8 m × 8 m 25 Km Quad Polarization Standard mode 25 m × 25 m 100 Km Single or Dual Polarization Wide mode 30 m × 30 m 15 Km Single or Dual Polarization ScanSAR Narrow mode 50 m × 50 m 300 km Single or Dual Polarization ScanSAR Wide mode 100 m × 100 m 100 m Single or Dual Polarization
Sentinel-1A/1B constellation	C-band at 5.405 GHz	2014–Present (S-1A) 2016–Present (S-1B)	6 days	Stripmap mode 5 m × 5 m 80 km Single or Dual Polarization Interferometric Wide Swath (IW) mode 5 mx 20 m 250 km Single or Dual Polarization Extra Wide Swath mode 20 m × 40 m 400 km Single or Dual Polarization Wave mode 5 m × 5 m 20 Km Single Polarization
TerraSAR-X/ TanDEM-X	X-band at 9.65 GHz	TSR-X (2007–Present) TDM-X (2010–Present)	11 days	Staring SpotLight (ST) mode 0.6 m × 0.24 m 4 Km × 3.7 Km Single Polarization High Resolution SpotLight 300 MHz (HS300) mode 0.6 m × 1.1 m 10 Km × 5 Km Single Polarization High Resolution SpotLight (HS) mode 1.2 m × 1.1 m or 1.2 m × 2.2 m 10 Km × 5 Km Single or Dual Polarization SpotLight (SL) mode 1.2 m × 1.7 m or 1.2 m × 3.4 m 10 Km × 10 Km Single or Dual Polarization StripMap (SM) mode 1.2 m × 3.3 m or1.2 m × 6.6 m 30 Km × 50 Km (Single-pol) & 15 Km × 50 Km (Dual-pol) Single or Dual Polarization ScanSAR (SC) mode 1.2 m × 18.5 m 100 Km × 150 Km Single Polarization Wide ScanSAR (WS) mode 1.7 m–3.3 m × 18.5 m 270 Km × 200 Km Single Polarization
Cosmo SkyMED Constellation	X-band at 9.65 GHz	CSMD(1)-2007–Present CSMD(2)-2007–Present CSMD(3)-2008–Present CSMD(4)-2010–Present	4 days	Spotlight mode 1 m × 1 m 10 Km Single Polarization (HH or VV) Stripmap: Himage mode 3 m × 3 m 40 Km Single Polarization (HH or HV or VH or VV) Stripmap: PingPong mode 15 m × 15 m 30 Km Dual Polarization (HH + VV or HH + HV or VV + VH) ScanSAR: Wide Region Mode 30 m × 30 m 100 Km Single Polarization (HH or HV or VH or VV) ScanSAR: HugeRegion Mode 100 m × 100 m 200 Km Single Polarization (HH or HV or VH or VV)

Table A2. Upcoming Missions SAR applicable in remote sensing applications of snow.

Satellite Sensor	Operating Frequency Band	Operation Period	Temporal Repeatability	Operational Imaging modes Resolution(range x azimuth) Swath covered (km) Polarizations
ALOS-PALSAR 3	L Band at 1.27 GHz	Proposed 2021–2028	14 days	Spotlight mode 1 m × 3m 35 Km Single, Dual Polarizations Stripmap mode 3/6/10 m 100–200 Km Single, Dual, Compact, Quad Polarizations ScanSAR mode 25 m 700 Km Single, Dual, Compact, Quad Polarizations
NISAR	L-band at 1.25 GHz S-band at 3.2 GHz	Proposed 2022–2025	12 days	L-Band SweepSAR Mode 3–10 m resolution 240 km swath Single, Dual, Compact, Quad Polarizations S-Band SweepSAR Mode 3–10 m resolution 240 km swath Single, Dual, Compact, Quad Polarizations
Radar Constellation Mission (RCM)	C-Band at 5.405 GHz	2019–2026	Daily coverage	500 km swath 5 m–50 m resolution Single, Dual, Compact, Quad Polarizations
Tandem-L	L-band at 1.25 GHz	Proposed 2022–2032	16 days	Staggered SAR imaging mode is proposed 1 m resolution with 50 km swath, 7 m resolution with 350 km swath